MBE Advance Access published April 10, 2012

Fast Molecular Evolution Associated with High Active Metabolic Rates in Poison Frogs

Juan C. Santos*[,1,2,3]

[1]Section of Integrative Biology, The University of Texas at Austin

[2]Texas Memorial Museum, The University of Texas at Austin

[3]National Evolutionary Synthesis Center, Durham, North Carolina

***Corresponding author:** E-mail: juan.santos@duke.edu.

Associate editor: Koichiro Tamura

Abstract

Molecular evolution is simultaneously paced by mutation rate, genetic drift, and natural selection. Life history traits also affect the speed of accumulation of nucleotide changes. For instance, small body size, rapid generation time, production of reactive oxygen species (ROS), and high resting metabolic rate (RMR) are suggested to be associated with faster rates of molecular evolution. However, phylogenetic correlation analyses failed to support a relationship between RMR and molecular evolution in ectotherms. In addition, RMR might underestimate the metabolic budget (e.g., digestion, reproduction, or escaping predation). An alternative is to test other metabolic rates, such as active metabolic rate (AMR), and their association with molecular evolution. Here, I present comparative analyses of the associations between life history traits (i.e., AMR, RMR, body mass, and fecundity) with rates of molecular evolution of and mitochondrial loci from a large ectotherm clade, the poison frogs (Dendrobatidae). My results support a strong positive association between mass-specific AMR and rates of molecular evolution for both mitochondrial and nuclear loci. In addition, I found weaker and genome-specific covariates such as body mass and fecundity for mitochondrial and nuclear loci, respectively. No direct association was found between mass-specific RMR and rates of molecular evolution. Thus, I provide a mechanistic hypothesis of the link between AMRs and the rate of molecular evolution based on an increase in ROS within germ line cells during periodic bouts of hypoxia/hyperoxia related to aerobic exercise. Finally, I propose a multifactorial model that includes AMR as a predictor of the rate of molecular evolution in ectothermic lineages.

Key words: molecular evolution, metabolic rates, life history, ectotherms, path analysis.

Introduction

Molecular evolution is paced by the combined effects of mutation rate, genetic drift, and natural selection (Graur and Li 2000). Likewise, the rate of the accumulation of nucleotide changes per unit of time also correlate with life history traits including physiological attributes at both organismal and cellular levels (Martin and Palumbi 1993; Bromham and Penny 2003; Gillooly et al. 2005). For instance, small body size, rapid generation time, production of reactive oxygen species (ROS), and high basal metabolic rates (BMRs or RMRs from ectotherms) are hypothesized to correlate with higher rates of molecular substitution (Welch et al. 2008; Galtier et al. 2009). However, recent studies have shown contradictory evidence about such associations. For example, faster generation times tend to be correlated with higher rates of molecular evolution in invertebrates (Thomas et al. 2010), but BMRs have been found to be independent of the speed of molecular evolution in both ectotherm and endotherm vertebrates if phylogeny is accounted (Lanfear et al. 2007; Nabholz et al. 2008). Other physiological parameters, such as active metabolic rates (AMRs), have not been tested for their associations with molecular evolution.

Metabolism or energy flux within an organism relates growth, reproduction, and self-maintenance (Karasov and Martinez del Rio 2007). RMRs represent the lowest bound of the metabolic budget, whereas AMRs constitute the upper limit achieved at the highest physical activity (Schmidt-Nielsen 1984). Another related parameter is aerobic scope (hereafter Scope), which is an adjusted measurement of AMR (i.e., Scope = AMR − RMR). AMR and Scope are proxies of the athletic prowess and measure the targeted oxygen supply to muscles during forced activity (Gatten et al. 1992; Bishop 1999). Most organisms function with an average metabolic rate (called field metabolic rate [FMR]), which is a mean energetic cost of life cycle activities during a day (e.g., growth, sleep, digestion, reproduction, and escaping predation). Therefore, FMR might be considered to be closer to AMR than to RMR (Butler et al. 2004; Nagy 2005; Hillman et al. 2009).

All metabolic rates measure energy production in the form of heat at different levels of physical activity (Schmidt-Nielsen 1984). The chief mechanism of energy production is cell respiration; however, this process is not completely efficient and generates mutagenic byproducts such as ROS (Galtier et al. 2009). Accordingly, oxidative stress is defined as the damage resulting from injuries inflicted by ROS and other nonradicals, such as reactive aldehydes and singlet oxygen (Yu 2005; Monaghan et al. 2009). Mutation rates are assumed to reflect the causal

effect of oxidative stress in the form of DNA damage (Martin and Palumbi 1993). Yet, other life history traits, including body mass, generation time, fecundity, and DNA repair mechanisms, also influence, alone or in combination, the rates of molecular evolution (Brown et al. 2000, 2004; Bromham 2009, 2011).

At least three main hypotheses were proposed to explain the variability in rates of molecular evolution among genes and lineages. However, none of these hypotheses explain all the variation in molecular evolution rates by a single predictor; instead, they suggest a set of likely covariates causing a synergistic effect on rates (Bromham 2011). The generation time hypothesis suggests an inverse association between the time of reproduction and the substitution rates in germ line DNA (Ohta 1993; Smith and Donoghue 2008; Thomas et al. 2010). This model implies that higher rates of molecular evolution are associated with shorter generation times and faster accumulation of DNA replication errors per unit of time (Bromham et al. 1996). Evidence consistent with this hypothesis includes shorter generation times associated with faster mutation rates (e.g., higher synonymous dS substitution rates) in mammals (Bromham et al. 1996; Welch et al. 2008). Even though the generation time hypothesis is supported in some invertebrate lineages (Thomas et al. 2010), its generality across ectotherms is unknown.

The longevity hypothesis inversely relates the length of lifespan and the age at the onset of senescence with the rate of molecular evolution (Nabholz et al. 2008). This hypothesis predicts higher substitution rates in early reproducing lineages, mitochondrial genomes, and nonfunctional domains of protein-coding genes (Bromham 2011). In contrasts, late reproducing organisms are expected to have adaptations for efficient DNA repair and management of free radicals (Galtier et al. 2009). Evidence in favor of this hypothesis includes long-lived endotherms that have better DNA maintenance (e.g., higher tumor suppression and reduced telomerase activity), lower ROS production, slower mitochondrial decay, and larger body sizes (Bromham 2011). Extensive phylogenetic studies are required to test the generality of the longevity hypothesis in ectotherms.

Finally, the metabolic rate hypothesis states that the pace of molecular evolution is correlated with the production of free radicals (e.g., ROS) during oxidative cell respiration (Martin and Palumbi 1993). This hypothesis assumes that variation in RMRs should positively correlate with the levels of ROS and the rates of molecular evolution (Martin et al. 1992; Gillooly et al. 2005). Several lines of evidence support the metabolic rate hypothesis: endotherms have much higher rates than ectotherms (Martin 1999), species with high mass-specific RMRs have greater DNA repair rates (Foksinski et al. 2004), high mutation rates in mitochondrial DNA is explained by its closeness to the site of aerobic respiration (Rand 1994), and senescence is associated with ROS production and mitochondrial decay (Ricklefs 2008). However, phylogenetic comparative analyses have challenged the association of RMRs with the rates molecular evolution in ectotherms and endotherms (Seddon et al. 1998; Lanfear et al. 2007; Bromham 2009). To my knowledge, no comparative analyses have tested the association between other metabolic rates (i.e., AMRs or FMRs) and the rates of molecular evolution.

To test if AMRs are associated with genome-wide increases in molecular evolution rates, I compiled data on metabolic rates (AMR and RMR), life history (i.e., body mass and clutch size), rates of molecular evolution (nuclear and mitochondrial), and phylogenetic relationships of a large ectotherm lineage, the poison frogs (Dendrobatidae). These Neotropical amphibians form a widespread clade of approximately 285 species with diverse biological characteristics such as parental care, aposematism, and metabolic rates (Summers 2000; Santos et al. 2003; Santos and Cannatella 2011). Here, due to the generality of the main question (i.e., Are AMRs associated with genome-wide increases in molecular evolution rates?), I explored three main hypotheses based on the complexity and location of the employed molecular markers. Specifically, I tested if AMR and other life history traits predict rates of molecular evolution of 1) RNA-coding stem–loop mitochondrial genes (e.g., ribosomal and tRNAs), 2) mitochondrial protein-coding genes, and 3) nuclear protein-coding genes.

To answer these specific questions, I used single predictor and multivariate phylogenetic comparative methods. Three approaches were employed, namely, 1) relative rate tests (RRTs) using pairs of sister species (Bromham et al. 2000), 2) phylogenetic generalized least squares (PGLS) on absolute rates of molecular evolution (Lanfear et al. 2010), and 3) phylogenetic path analysis based on independent contrasts (Santos and Cannatella 2011) and Bayesian analyses (Lartillot and Poujol 2011) to estimate variance–covariance (VCV) matrices of life history traits on absolute rates, synonymous substitution (dS) rates, and ω (i.e., ratio of nonsynonymous to synonymous substitutions or dN/dS).

Materials and Methods

Metabolic Rates, Body Mass, and Fecundity Data

Life history and metabolic rate parameters of 54 species of poison frogs were compiled from Santos and Cannatella (2011) (supplementary tables 1 and 2, Supplementary Material online). The included variables were 1) resting metabolic rate (RMR, oxygen consumption while resting or VO_2 rest consumed $\times$ h^{-1}); 2) AMR after nonsustainable exercise (AMR, oxygen consumption after forced activity or VO_2 active consumed $\times$ h^{-1}); 3) Scope calculated as the difference between AMR and RMR (Gatten et al. 1992); 4) mean body mass to the nearest 0.01 g of all the individuals tested in the metabolic experiments; and 5) a proxy for fecundity (i.e., clutch size) estimated by the maximum number of eggs per clutch, mature oocytes per female, or back-riding tadpoles carried by nursing parent because most dendrobatid species transport their entire progeny at once (Wells 2007). However, true fecundity should be defined as the maximum number of potential progeny (Hamilton 2009).

All the physiological data were measured from a total of 474 adult individuals at 24.5–25.5 °C under the guidelines of an animal care permit (IACUC # 05111001). Details of the physiological experiments were previously described including capture, handling, and metabolic rate estimation (Santos and Cannatella 2011). From the physiological raw data, mass-specific metabolic rates (AMR, RMR, and Scope) were estimated by dividing raw metabolic rates by the body mass of each individual. The average of all conspecific individual rates was used as the species mass-specific metabolic rate in the bivariate and multivariate comparative analyses. Body mass, fecundity, and mass-corrected metabolic rates were transformed using natural logarithms to improve the data distribution as required by the comparative analyses of rates of molecular evolution (e.g., to meet the requirement that variances of life history trait differences were not related to their absolute values) (Lanfear et al. 2010).

Molecular Data

The sequence alignments included the 54 species for which metabolic rates were measured with the exception of the ND1 gene sequence of *Allobates juanii*. The supermatrix included both mitochondrial (total mtDNA ~ 5.5 kb) and nuclear loci (total nuclear DNA ~ 5.0 kb). The analyzed mitochondrial genes were 12S and 16S rDNAs; valine, leucine, and methionine tRNAs (tRNAs V–L–M); NADH subunit 1 (*ND1*); NADH subunit 2 (*ND2*); and cytochrome *b* (*CYTB*). The nuclear data included protein-coding segments of the following genes: brain-derived neurotrophic factor (*BDNF*), bone morphogenetic protein 2 (*BMP2*), NCX1 sodium-calcium exchanger 1 (*NACA*), 3′-nucleotidase (*NT3*), proopiomelanocortin A (*POMC*), tyrosinase precursor (*TYR*), and zinc finger E-box binding homeobox 2 (*ZFX*). All sequences were validated by comparison with other anuran sequences using NCBI BLAST as previously suggested (Santos et al. 2009). Details of polymerase chain reaction amplifications and sequencing of individual fragments were described elsewhere (Santos and Cannatella 2011), GenBank accession numbers are given in supplementary table 3 (Supplementary Material online), and all sequence alignments are deposited at http://datadryad.org/. The concatenated supermatrix from all the genes included a total of 8,517 unambiguously aligned characters and was used to estimate the phylogeny of poison frogs.

Supermatrix Tree Estimation

The supermatrix phylogeny was analyzed under a partitioned by gene approach. The model of nucleotide substitution from each partition was determined using ModelTest v. 3.7 (Posada and Crandall 1998; Posada and Buckley 2004), and all gene and partition matrices favored complex models approximated by GTR + Γ + I without significant over-parametrization (Lemmon and Moriarty 2004) (see supplementary tables 4 and 5, Supplementary Material online). The supermatrix maximum likelihood (ML) tree was estimated using a genetic algorithm in GARLI v. 0.960 (Zwickl 2006) and sequential and parallel ML-based inferences in RAxML v. 7.0.4 (Stamatakis 2006). For each methodology, a total of 30 independent runs were used to infer the best tree, and 500 nonparametric bootstrap searches determined the support of the nodes. Both programs gave similar topologies; the RAxML phylogeny was used for all the comparative analyses and is deposited at http://datadryad.org/. A complementary Bayesian phylogenetic inference was performed using MrBayes v. 3.4 (Huelsenbeck and Ronquist 2001) with default settings for all priors. The Markov Chain Monte Carlo (MCMC) setup included four independent runs, each one with four chains of 50 million generations with a sampling rate every 1,000 generations. The convergence of the runs was determined using Tracer v. 1.4 (Rambaut and Drummond 2007). Approximately, 30,000 trees were discarded as burnin. The supermatrix phylogeny did not significantly differ from previous studies (Santos et al. 2003, 2009) with the exception of Clade C and B as sister lineages (fig. 1). The taxonomic nomenclature of poison frogs was based on the unequivocal monophyly of Dendrobatidae, and *Dendrobates* was considered a single genus (Santos et al. 2009).

Single-Predictor Phylogenetic Comparative Analyses

Two single predictor approaches were used for the comparative analyses. These include a (tables 1 and 2) RRT using pairs of sister species (Bromham et al. 2000) and PGLS correlation analyses (Martins and Hansen 1997; Pagel 1997) on absolute rates of molecular evolution (Lanfear et al. 2010). For the RRT, branch lengths were assumed to represent the number of substitutions since the divergence form a common ancestor (Lanfear et al. 2007). Due to the complexity and diversity of the molecular markers employed, three sets of particular genes were defined based on marker characteristics: mitochondrial RNA-coding stem–loop genes (i.e., 12S, 16S, and tRNAs); concatenated mitochondrial protein-coding genes (i.e., *CYTB*, *ND1*, and *ND2*); and concatenated nuclear protein-coding genes (i.e., BDNF, *BMP2*, *NACA*, *NT3*, *POMC*, *TYR*, and *ZFX*). The RRT method included the following steps: 1) the model of nucleotide substitution from each matrix was determined using ModelTest v. 3.7 (supplementary tables 4 and 5, Supplementary Material online) (Posada and Crandall 1998; Posada and Buckley 2004); 2) individual stem–loop mitochondrial genes, concatenated mitochondrial protein-coding, and concatenated nuclear protein-coding branch lengths were estimated over the constrained supermatrix RAxML topology using Paup v. 4.0 (Swofford 2000); 3) each pair of sister species was considered as a single independent contrast (Bromham et al. 2000); 4) the comparisons included only taxa with branch lengths <1.0 to ensure that saturated points are excluded from the analyses; 5) the independent variables corresponded to any of the analyzed life history traits (i.e., mass-specific RMR, mass-specific AMR, mass-specific Scope, body mass, and fecundity) calculated as ln (T_1/T_2), where T_1 was the trait value for species 1, T_2 was the trait value for species 2, the assignation to either T_1 or T_2 was randomized (Lanfear et al. 2007); 6) the dependent variable (i.e., branch length) was calculated as ln (L1/L2), where L1 was the branch length of species 1, L2 was

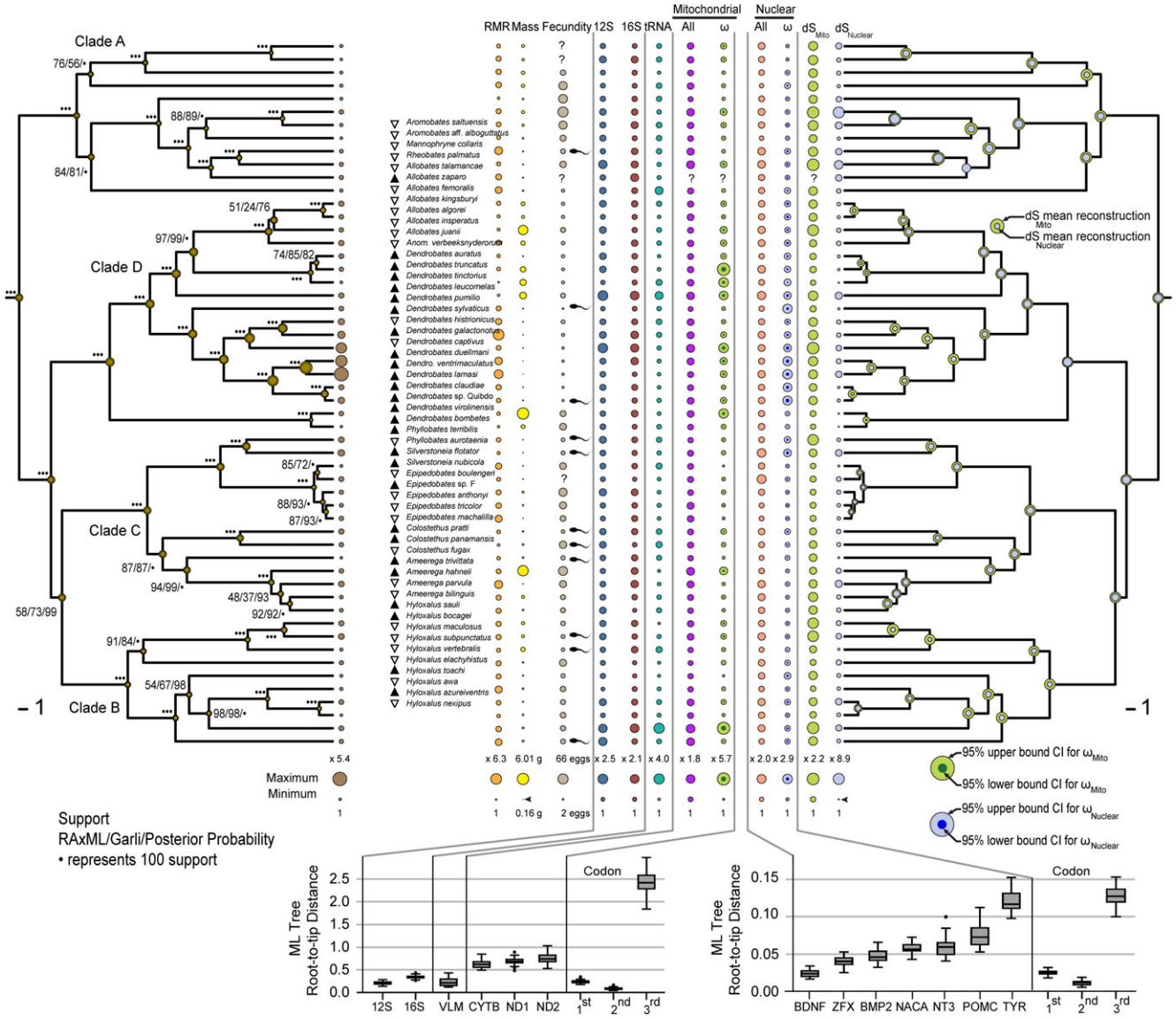

FIG. 1. Poison frog phylogeny, life history traits, absolute rates of molecular evolution, ω (dN/dS), and dS rates at terminal branches for mitochondrial and nuclear loci. Circles represent an area proportional to each life history variable, including its maximum and minimum values. AMR (right tree) and dS rates (left tree) are the reconstructions of ancestral states. Fecundity indicates the largest number of eggs per clutch or back-riding tadpoles (tadpole sign) per species. Box plots are the distribution of the root-to-tip distances of the ML tree for each molecular segment analyzed. Mass-specific AMR values above or below all species mean are indicated (i.e., ▲ = high AMR and ∇ = low AMR, respectively). Support values in the phylogeny correspond to the summary of 500 ML nonparametric bootstraps estimated with GARLI (left), RAxML (center), and posterior probabilities (right). (●) represents 100% of nodal support.

the branch length of species 2, and the assignation followed the order of the independent variable (Lanfear et al. 2007), and this logarithmic transformation was required to meet the assumption that the variance of life history traits and rates differences increases linearly with evolutionary time (Lanfear et al. 2010); 7) each comparison pair was scored as "+" or success if the sign of the difference in the life history trait and branch length were identical and as "−" or failure, if otherwise; 8) the process was iterated again starting from step 3) after pruning species pairs whose contrasts were already calculated; 9) the iterative process was repeated until the maximum number of species pairs was attained (Brown and Pauly 2005); 10) to ensure that sufficient information was available, the test of Welch and Waxman was used to identify and exclude shallow contrasts from the analyses (Welch and Waxman 2008); 11) nonparametric sign tests were performed between the observed sign scores against a null hypothesis of equal number of "+" and "−" signs (i.e., H_0: $P = 0.5$ vs. H_1: $P \neq 0.5$) and P values were reported with a significance level of $\alpha = 0.05$ for a two-sided distribution; and 12) due to the multiple testing, a false discovery rate (FDR) procedure was required to identify the expected proportion of false positives among all significant results. The FDR procedure has been previously described (Benjamini and Hochberg 1995) as follows: for $H_1, H_2, \ldots, H_m$ hypotheses based on corresponding P values such as $P_1, P_2, \ldots, P_m$; let $P_{(1)} \leq P_{(2)} \leq \ldots \leq P_m$ be the ordered P values; define $H_{(i)}$ as the null hypothesis

Table 1. Results of the Sign Test on Branch Lengths and PGLS between Molecular and Life History Variables of Poison Frogs.

		RMR (Mass Specific)				AMR (Mass Specific)				Mass				Fecundity[a]			
Gene/Codon/Substitution		+/−	P_{Sign}	λ	r_{PGLS}	+/−	P_{Sign}	λ	r_{PGLS}	+/−	P_{Sign}	λ	r_{PGLS}	+/−	P_{Sign}	λ	r_{PGLS}
Mitochondrial	12S	(10/10)	1.00	0.64	−0.03	(13/7)	0.26	0.72	0.40**	(8/12)	0.50	0.63	−0.02	(9/8)	1.00	0.93	0.08
	16S	(11/8)	0.65	0.71	0.21	(10/9)	1.00	0.70	0.32*	(10/9)	1.00	0.65	0.13	(8/8)	1.00	0.92	0.05
	tRNA	(9/9)	1.00	0.68	−0.19	(6/12)	0.24	0.73	−0.18	(11/7)	0.48	0.64	0.09	(6/9)	0.61	0.92	−0.16
	Protein coding	(10/10)	1.00	0.59	0.15	(11/9)	0.82	0.70	0.41**	(10/10)	1.00	0.66	0.18	(8/8)	1.00	0.90	0.14
	dN	(13/8)	0.38	0.76	−0.22	(11/10)	1.00	0.69	−0.05	(11/10)	1.00	0.69	0.22	(8/9)	1.00	0.95	0.15
	dS	(7/8)	1.00	0.74	−0.18	(9/6)	0.61	0.67	−0.09	(6/9)	0.61	0.67	0.14	(5/7)	0.77	0.96	0.19
Nuclear	Protein coding	(11/11)	1.00	0.65	0.04	(18/4)	<0.01**	0.63	0.38**	(9/13)	0.52	0.63	−0.02	(9/9)	1.00	0.92	0.02
	dN	(10/11)	1.00	0.75	−0.25	(14/7)	0.19	0.66	−0.15	(13/8)	0.38	0.67	0.21	(8/9)	1.00	0.97	0.30*
	dS	(10/11)	1.00	0.65	0.03	(15/6)	0.08	0.67	0.39**	(10/11)	1.00	0.58	−0.27	(9/8)	1.00	0.90	−0.13

NOTE.—P_{Sign} values and P values for PGLS are two-tailed, the significance is given by * if $0.05 > P > 0.01$ and ** if $P < 0.01$. After the FDR procedure, no P values were rejected.
[a] Fecundity is determined by a proxy, clutch size.

corresponding to $P_{(i)}$; then the FDR procedure is determined as follows; let k be the largest i for which $P_{(i)} \leq \frac{i}{m}q^*$, then reject all $H_{(i)}$ $i = 1, 2, \ldots, k$; where q^* was significant at the $\alpha = 0.05$ level for a one-sided distribution.

In a complementary analysis, branch lengths based on dN and dS substitutions were determined from concatenated mitochondrial and nuclear protein-coding sequences. Branch lengths were estimated with a free ω for each branch across the phylogeny using CODEML module of PAML v. 4.3 (Yang 2007). The following parameter alternatives of PAML were used: 1) without assuming a molecular clock (clock: 0); 2) with codon frequencies estimated from the average nucleotide frequencies at the three codon positions (CodonFreq: 2); 3) including all sites (cleandata: 0); 4) ω ratio free to vary across the tree (model: 1, NSsites: 0, and fix_omega: 0). Branch length estimations were run three times with three starting values of ω (i.e., 0.4, 1.0, and 2.4) to avoid problems arising from local optima (Yang and Nielsen 1998). The same described RRT procedure (see previous paragraph) was used to determine the associations between life history traits with dN and dS branch lengths.

A clarification needs to be made to explain why the use of only extant sister pairs was not warranted for poison frogs. First, these frogs are a recent monophyletic clade of approximately 40 Ma (Santos et al. 2009), and the expected number of substitutions is far less than in older groups common in RRT analyses (e.g., Arthropoda, Aves, Mammalia, or Mollusca). Second, several of the sister taxa from the concatenated nuclear matrix were excluded for being shallow contrasts after the Welch and Waxman test. These exclusions reduced the total number of sister pairs to less than half, consequently, reducing the power of sign tests and the ability to detect underlying patterns in the data (Lanfear et al. 2010). Finally, the RRT is a single predictor test, and recent studies strongly advocate for more powerful multivariate analyses such as covariance analyses (Lartillot and Poujol 2011) and structural equation models (Santos and Cannatella 2011). These procedures convey multifactor inferences and reveal indirect relationships, which are better suited when dealing with covarying life history traits.

Table 2. Results of the Sign Test on Branch Lengths and PGLS between Molecular and Mass-Specific Scope of Poison Frogs.

		Scope (Mass Specific)			
Gene/Codon/Substitution		+/−	P_{Sign}	λ	r_{PGLS}
Mitochondrial	12S	(12/8)	0.50	0.72	0.43**
	16S	(11/8)	0.65	0.69	0.31*
	tRNA	(5/13)	0.10	0.72	−0.17
	Protein coding	(11/9)	0.82	0.72	0.41**
	dN	(11/10)	1.00	0.68	−0.03
	dS	(9/6)	0.61	0.66	−0.08
Nuclear	Protein coding	(19/4)	<0.01**	0.61	0.39**
	dN	(15/6)	0.08	0.65	−0.13
	dS	(16/5)	0.03*	0.66	0.40**

NOTE.—P_{Sign} values and P values for PGLS are two-tailed, the significance is given by * if $0.05 > P > 0.01$ and ** if $P < 0.01$. After the FDR procedure, no P values were rejected.

Absolute rates of molecular evolution per species were determined for the RNA-coding stem–loop mitochondrial genes, concatenated mitochondrial, and nuclear matrices using the method developed by Brown and Pauly (2005). The absolute rates were independent of time, and their estimation can be summarized in the following steps: 1) a user-specified starting ultrametric tree was estimated using the RAxML supermatrix topology under a penalized likelihood rate smoothing (Sanderson 2002) with the dendrobatid crown node set to 40.931 arbitrary units of time in TreeEdit v. 1.0 (Rambaut and Charleston 2002), and this number reflects the approximate age of Dendrobatidae in Ma (Santos et al. 2009); 2) the chronogram of each set was estimated using a relaxed clock model approach implemented in Beast v. 1.5.3 (Drummond and Rambaut 2007) with four user-defined priors, namely, a molecular model for each sequence group (supplementary tables 4 and 5, Supplementary Material online), the user-specified starting ultrametric tree, a normally distributed arbitrary age of the root (mean 40.931 and standard deviation [SD] 5.360) based on the age of Dendrobatidae (Santos et al. 2009), and an $U(0, 100)$ hyperprior for ucld.mean; 3) suggested modifications for default MCMC operators were determined after 2 runs of 2 million generations with a sampling rate every 1,000 generations; 4) the final

ultrametric trees were estimated with the suggested MCMC operator calibrations and 4 runs of 40 million generations sampled every 1,000 generations; 5) the convergence of the runs and the optimal burnin was determined using Tracer v. 1.4 (Rambaut and Drummond 2007); 6) the tree files were combined using LogCombiner (Drummond and Rambaut 2007), and approximately 20,000 initial trees were discarded as burnin; 7) the maximum clade credibility summary tree was determined with the retained trees using TreeAnnotator (Drummond and Rambaut 2007); and 8) the absolute rate of molecular evolution at each terminal branch (supplementary tables 6 and 7, Supplementary Material online) was obtained from a summary tree using FigTree v. 1.2.3 (Rambaut 2009).

Phylogenetic correlations between absolute rates of molecular evolution, dN, dS, and life history traits were determined using PGLS (Garland and Ives 2000; Rohlf 2001). This comparative method can be summarized as follows: 1) life history variables (body mass, fecundity, and rate of molecular evolution) were transformed using logarithms to improve their distribution (Garland 1992); 2) each trait was tested for phylogenetic signal by estimating its phylogenetic covariance coefficient Pagel's λ (Pagel 1993) using the "fitContinuous" function of the geiger R-package v. 1.3 (Harmon et al. 2008); Pagel's λ describes a tree transformation parameter that has the effect of gradually exclude underlying phylogenetic structure (Pagel 1993, 1999); 3) the significance of λ was determined against a null hypothesis of no phylogenetic signal (i.e., H_0: $\lambda = 0$) by contrasting ML scores using a likelihood ratio test (Harmon et al. 2008); 4) pairwise correlations were determined using the fit linear model using generalized least squares or the "gls" function of the nlme R-package v. 3.1 (Pinheiro et al. 2011) under a log-likelihood maximization (i.e., ML method) and a Pagel's λ correlation structure with a starting value of $\lambda = 1$ estimated using "corPagel" function of the ape R-package v. 2.7 (Paradis et al. 2004); and 5) the significance of each PGLS correlation coefficient was determined from the nmle R-package output with a significance α level set to 0.05 for a two-sided distribution.

Model Estimation of the Phylogenetic Path Analysis

A multivariate approach is necessary to account for the complex network of relationships between life history traits and rates of molecular evolution (Bromham 2011). My choice of path analysis is suitable for this task for the following reasons. First, path analysis allows the assessment of direct, indirect, and compound (i.e., mixture of direct and indirect) casual–covarying relationships among a set of observed variables (Kline 2005). Second, path analysis allows testing alternative models of causal relationships among traits by determining the magnitude of path connections, total variance explained of the dependent variables, and overall model fit (Scheiner et al. 2000; Grace 2006). Third, the available methodology for path analysis can easily be extended from phylogenetically corrected VCV matrices (Lartillot and Poujol 2011) and independent contrasts (Santos and Cannatella 2011).

To perform phylogenetic path models, two types of input data can be used, namely, a VCV matrix and Pagel's λ adjusted independent contrasts. The VCV matrix was estimated using the following approach: 1) the input data for Coevol v. 1.1 (Lartillot and Poujol 2011) were the life history trait variables (i.e., body mass, AMR, RMR, and fecundity; Scope was excluded due to collinearity with AMR), molecular alignments (i.e., concatenated mitochondrial or nuclear protein-coding genes), and user-defined tree (i.e., RAxML supermatrix topology); 2) to run Coevol, the age calibrations for the root the tree was set to a mean of 40.931 and a SD of 5.360 for the age of Dendrobatidae (Santos et al. 2009); the number of cycles for the MCMC was set to 4,000; to estimate the covariance matrix Σ_0, the default option was used that allows each entry along the diagonal of Σ_0 to be different and derived from the data (i.e., each using a truncated Jeffrey's prior); the geodesic averaging was used to compute branch specific mean values of the substitution parameter; the dS rates and ω were chosen to be included as molecular evolution variables in the VCV matrix; and the genetic code was set based on the input data (i.e., mammal mitochondrial or universal); 3) two separate chains were run to ensure convergence from independent starting points; 4) chain convergence and optimal burnin were determined using the tracecomp module of PhyloBayes v. 3.3 (Lartillot et al. 2009); and 5) the final VCV matrix and ancestral reconstructions were determined from retained samples using the readcoevol module of Coevol v. 1.1 (Lartillot and Poujol 2011). In complimentary set of runs (supplementary table 8, Supplementary Material online), the covariance matrix Σ_0 was determined using the $\Sigma_0 = \kappa I_M$ parametrization, where I_M is the identity matrix of size M where $M = K$ (substitution parameters) + L (life history traits), and κ is prior mean variance for each component of the multivariate process (Lartillot and Poujol 2011). I used κ prior equal to 1.0 to encompass the range of scales observed (i.e., main diagonal of the top matrices on table 4) for the rate of change of the substitution and life history traits (Lartillot and Poujol 2011). The resulting VCVs using the default parametrization (i.e., truncated Jeffrey's priors) and $\kappa = 1.0$ were input for the phylogenetic path analyses.

The estimation of the Pagel's λ adjusted independent contrasts (λ-PICs) can be summarized in the following steps: 1) the input data were life history variables (i.e., body mass, AMR, RMR, and fecundity) and absolute rates traits transformed using logarithms to improve their distribution (Garland 1992); 2) each trait was tested for phylogenetic signal under a RAxML supermatrix topology, and its specific Pagel's λ was determined using the "fitContinuous" function of the geiger R-package v. 1.3 (Harmon et al. 2008); 3) the branch lengths of the RAxML supermatrix tree were transformed in accordance to each trait λ (table 3); 4) λ-PICs were estimated using the transformed tree with the "pic" function of the ape R-package v. 2.7 (Paradis et al. 2004); and 5) the presence of multivariate λ-PIC outliers was determined by calculating Mahalanobis distances (Tabachnick and Fidell 2007), and no cases were found.

Table 3. Phylogenetic Path Analyses of Life History Variables with Ribosomal, tRNAs, and Protein-Coding Genes.

Initial Models (just-identified or saturated model)

	12SrDNA, 16SrDNA, and tRNAs							Combined Protein-Coding Genes						
Path Coefficients	RMR	AMR	Fecundity	12S	16S	$tRNA_{V-L-M}$	λ_{trait}	Path Coefficients	RMR	AMR	Fecundity	Mitochondrial	Nuclear	λ_{trait}
Mass	−0.41	−0.40	0.37	0.08	0.33	0.05	0.63	Mass	−0.41	−0.40	0.37	0.38	0.15	0.63
RMR	—	0.42	−0.17	−0.21	0.16	−0.14	0.64	RMR	—	0.42	−0.17	0.13	−0.14	0.64
AMR	—	—	−0.10	0.53	0.39	−0.09	0.68	AMR	—	—	−0.10	0.51	0.51	0.68
Fecundity	—	—	—	−0.01	−0.03	−0.19	0.92	Fecundity	—	—	—	0.08	−0.06	0.92
12S	—	—	—	—	0.48	0.45	0.00	Mitochondrial	—	—	—	—	0.15	0.00
16S	—	—	—	—	—	0.37	0.00	Nuclear	—	—	—	—	—	0.00
$tRNA_{V-L-M}$	—	—	—	—	—	—	0.00							
P values	RMR	AMR	Fecundity	12S	16S	$tRNA_{V-L-M}$	R_i^2	*P* values	RMR	AMR	Fecundity	Mitochondrial	Nuclear	R_i^2
Mass	<0.01	<0.01	<0.01	0.59	0.03	0.76	—	Mass	<0.01	<0.01	<0.01	<0.01	0.35	—
RMR	—	<0.01	0.23	0.14	0.29	0.39	—	RMR	—	<0.01	0.23	0.33	0.33	—
AMR	—	—	0.47	<0.01	<0.01	0.57	—	AMR	—	—	0.47	<0.01	<0.01	—
Fecundity	—	—	—	>0.99	0.86	0.21	—	Fecundity	—	—	—	0.53	0.64	—
12S	—	—	—	—	<0.01	<0.01	0.22	Mitochondrial	—	—	—	—	0.28	0.30
16S	—	—	—	—	—	<0.01	0.19	Nuclear	—	—	—	—	—	0.20
$tRNA_{V-L-M}$							0.07							

Final Models (constrained, path coefficients are in fig. 2)

	12SrDNA, 16SrDNA, and tRNAs (fig. 2A)							Combined Protein-Coding Genes (fig. 2B)						
P values[a]	RMR	AMR	Fecundity	12S	16S	$tRNA_{V-L-M}$		*P* values[a]	RMR	AMR	Fecundity	Mitochondrial	Nuclear	
Mass	<0.01	<0.01	0.01	*	*	*		Mass	<0.01	<0.01	0.01	<0.01	*	
RMR	—	<0.01	*	*	*	*		RMR	—	<0.01	*	*	*	
AMR	—	—	*	<0.01	<0.01	*		AMR	—	—	*	<0.01	<0.01	
Fecundity	—	—	—	*	*	*		Fecundity	—	—	—	*	*	
12S	—	—	—	—	<0.01	<0.01		Mitochondrial	—	—	—	—	*	
16S	—	—	—	—	—	<0.01		Nuclear	—	—	—	—	—	

NOTE.—Phylogenetic path analyses were performed using PICs for each trait estimated under trait specific Pagel's lambda (λ) tree transformation parameter. R_i^2 is the variance explained by the dependent variables in the initial model.

[a] *P* values of path coefficients of the final path model. Asterisk indicates that the path was constrained to be zero in the final model.

The λ-PICs were used as input data for the phylogenetic path analyses.

Four path models were estimated using VCVs and PICs. For the VCV-based models, life history traits were defined as predictors (i.e., exogenous variables) and mitochondrial or nuclear dS rates and ω as dependents (i.e., endogenous variables). Likewise, for the PICs-based models, life history traits were used as predictors of mitochondrial and nuclear absolute rates. Path model estimation can be summarized as follows: 1) a full initial (i.e., just-identified) model with all variables correlating to each other was estimated using MPlus v. 6.11 (Muthén and Muthén 2011) with VCV or PICs as input, ML as estimator with 2,000 iterations, including modification indices, and estimating standardized path coefficients; for the PICs, an extra step was necessary such that all variable intercepts were constrained to 0 (i.e., forced through the origin) as required for PICs statistical interpretation (Felsenstein 1985; Garland et al. 1992); 2) the initial output was explored and all nonsignificant path coefficients at an $\alpha = 0.05$ were identified; these initial path models are full multiple phylogenetic regression models, and their results were also reported; 3) a set of alternative path models were tested that constrained all or a combination of the nonsignificant paths (i.e., overidentified models); 4) the best-fitting model was selected based on several criteria (Santos and Cannatella 2011), namely, nonsignificant χ^2 supporting that the implied VCV matrix $\hat{\Sigma}_0$ is not statistically different from the observed VCV matrix Σ_0, overall parsimony (i.e., the model that has the less possible number of parameters to estimate without rejecting Σ_0), and good model fit indices including Bentler's comparative fit index (CFI, Bentler 1990), Tucker–Lewis index (TLI, Tucker and Lewis 1973), root mean square error of approximation (RMSEA, Browne and Cudeck 1993), and standardized root mean square residual (SRMR, Bentler 1995). The interpretation of model fit indices follows standard recommendations of model optimality including CFI > 0.95, TLI > 0.95, RMSEA < 0.05, and SRMR < 0.10 (Hu and Bentler 1999). Path models based on the VCVs with the $\kappa = 1.0$ parametrization were similar to those based using a truncated Jeffrey's prior, and they are presented in the supplementary fig. 1 and table 8 (Supplementary Material online).

Results

Variability in Life History Traits and Molecular Evolution Rates

The rates of molecular evolution and the life history traits showed a significant variation across the 54 species studied (fig. 1 and supplementary tables 1 and 2, Supplementary

Material online). Moreover, different rates of molecular substitution were evidenced between nuclear and mitochondrial loci. The mitochondrial genes evolved approximately 10 times faster than the nuclear loci, but the substitution rates were comparable to those of other ectotherms (Hoeeg et al. 2004; Townsend et al. 2008). Similarly, the codon positions and the synonymous sites of the mitochondrial genes evolved faster (i.e., ~16 times faster) than those corresponding to the nuclear loci. Estimates of dS and ω for mitochondrial and nuclear concatenated matrices also showed significant variation across the phylogeny. As expected, tRNAs, second codon positions, and dN substitutions showed the slowest rates of molecular evolution among the analyzed gene sequences.

Regarding life history traits, a significant variation was observed across the poison frog phylogeny (fig. 1 and supplementary tables 1 and 2, Supplementary Material online). Body mass showed a 30-fold difference between the smallest (~0.2 g) versus the largest (~6.0 g) species. Likewise, clutch size had a significant variation from lineages with few eggs (e.g., *Dendrobates* with 2 to 4 eggs per clutch) to several lineages with 2 to 33 times larger clutch sizes (e.g., *Hyloxalus* and *Allobates* with 8 and 66 eggs per clutch, respectively). Similarly, the metabolic parameters also showed a significant variation among lineages. For instance, RMRs had a significant variation across the poison frog phylogeny with a 6-fold difference between the lowest versus the highest values. Similarly, AMRs had a 5-fold difference between the lowest versus the highest values. However, AMRs had an uneven distribution across the phylogeny because some clades included the majority of the 27 species with high AMR (i.e., species with mass-specific AMR values above the mean of all estimates, in fig. 1). Specifically, Clade D had approximately 56% or 15/27 species with high AMR, Clade C had approximately 26% or 7/27, and Clade B had approximately 14% or 4/27, whereas Clade A had only approximately 4% or 1/27 species with high AMR. Likewise, ancestral reconstructions showed a rapid increase of AMR in Clade D in comparison to the rest of the family. Measurements based on Scope were similar to those based on AMR (supplementary tables 1 and 2, Supplementary Material online). Overall, the life history data showed a significant variation across the poison frogs with Clade D concentrating most of the high AMRs species.

Evidence of Higher Rates of Molecular Evolution Using Single Predictors

The results of the RRT and PGLS based on absolute rates (tables 1 and 2) suggest increases in the rates of molecular evolution in association with specific life history traits. Both RRT and PGLS results supported that AMR and Scope predict a significant ($P < 0.05$) positive association with the rates of molecular evolution of nuclear loci (i.e., substitutions per site and absolute rates). Likewise, RRT and PGLS also supported a significant ($P < 0.05$) positive association between Scope (i.e., adjusted measurement of AMR) with dS substitutions in nuclear genes. Only the PGLS analyses found a significant positive association ($P < 0.05$) of AMR and Scope with absolute rates of both RNA-coding and coding mitochondrial genes. In addition, the PGLS analyses also found a significant positive association ($P < 0.05$) between fecundity and dN substitutions in nuclear genes. In contrast, no evidence ($P > 0.05$) was found of associations between molecular evolution and RMR and body mass. Therefore, AMR and Scope are the only consistent single predictors of rates of molecular evolution in poison frogs.

Interpretation of the Phylogenetic Path Analyses on Rates of Molecular Evolution

Path analysis represents a multivariate hypothesis of causal and covariant effects among a set of variables. The initial estimates are just-identified models in which all VCVs are known, and they have zero degrees of freedom (i.e., the number of free parameters is equal to the number of known values). The tops of tables 3 and 4 provide just-identified model parameters including path coefficients (i.e., standardized regression coefficients), their significance, and total explained variance by the just-identified model (R_I^2) about the dependent variables. The interpretation of the just-identified model is a full multiple regression model, but more parsimonious models exist with fewer parameters to be estimated (i.e., over-identified models with degree of freedom > 0).

The final model path diagrams are provided in figure 2*A*–*D*, and the significance of each path coefficient is provided on tables 3 and 4. The elements of the path diagram and their interpretation are similar to those of structural equation models (Santos and Cannatella 2011), and they are summarized as follows. All the variables that were directly measured are represented within boxes. Error variables, indicated by *E*, represent unexplained variance derived from the combined effects of unseen covariates or measurement error. In all the models of figure 2, the dependent variables have significant ($P < 0.05$) error variables indicated by *E**. These results suggest that a significant fraction of the variance of the rates of molecular evolution might be explained by unaccounted life history covariates (e.g., longevity or generation time variables) excluding measurement error.

Paths are indicated by connecting arrows, and their magnitude is presented by standardized regression coefficients (i.e., values within oval shapes). A direct path between two variables represents a direct effect that cannot be explained through any other variable in a model. In the standard terminology of path analysis, direct effects should be understood as proposals of direct causal relationship between variables (i.e., independent on dependent) given all the observed variables included in a model (Alwin and Hauser 1975; Kline 2005; Grace 2006). Direct effects are indicated by single-headed arrows connecting one predictor (independent or exogenous) with a dependent (endogenous) variable (e.g., fig. 2*B*: AMR → nuclear with a magnitude of 0.40). Covariances are indicated by double-headed arrows connecting two variables (e.g., fig. 2*B*: mass ↔ AMR with a magnitude of −0.38). The absence

Table 4. Phylogenetic Corrected Covariances Using Truncated Jeffrey's Prior, Correlations, Posterior Probabilities, and *P* Values of Path Coefficients of Life History Variables with Nuclear and Mitochondrial Protein-Coding Genes Using a Multivariate Brownian Process and (dS, ω = dN/dS) Parametrization to Estimate Covariances.

Initial Models (just-identified or saturated model)

	Mitochondrial Protein-Coding Genes						Nuclear Protein-Coding Genes						
VCV	Mass	RMR	AMR	Fecundity	dS	ω	VCV	Mass	RMR	AMR	Fecundity	dS	ω
Mass	1.43	−0.24	−0.15	0.34	−0.02	0.52	Mass	1.49	−0.23	−0.19	0.32	−0.12	−0.12
RMR	—	0.29	0.09	−0.08	0.01	−0.04	RMR	—	0.37	0.11	−0.11	0.07	0.03
AMR	—	—	0.27	−0.05	0.06	0.22	AMR	—	—	0.30	0.01	0.31	0.09
Fecundity	—	—	—	0.64	−0.01	0.09	Fecundity	—	—	—	0.77	0.19	−0.11
dS	—	—	—	—	0.14	0.05	dS	—	—	—	—	0.66	0.10
ω	—	—	—	—	—	0.84	ω	—	—	—	—	—	0.26
Correlation	Mass	RMR	AMR	Fecundity	dS	ω	Correlation	Mass	RMR	AMR	Fecundity	dS	ω
Mass	—	−0.36	−0.24	0.35	−0.05	0.46	Mass	—	−0.31	−0.28	0.30	−0.12	−0.19
RMR	—	—	0.31	−0.19	0.07	−0.07	RMR	—	—	0.33	−0.20	0.13	0.10
AMR	—	—	—	−0.11	0.30	0.46	AMR	—	—	—	0.00	0.70	0.32
Fecundity	—	—	—	—	−0.03	0.12	Fecundity	—	—	—	—	0.26	−0.25
dS	—	—	—	—	—	0.16	dS	—	—	—	—	—	0.23
R_i^2	—	—	—	—	0.10	0.58	R_i^2	—	—	—	—	0.56	0.18
Posterior Probability[a]	Mass	RMR	AMR	Fecundity	dS	ω	Posterior Probability[a]	Mass	RMR	AMR	Fecundity	dS	ω
Mass	—	<0.01	0.05	0.99	0.41	0.97	Mass	—	0.01	0.02	0.99	0.31	0.29
RMR	—	—	0.99	0.08	0.63	0.38	RMR	—	—	0.99	0.08	0.74	0.63
AMR	—	—	—	0.23	0.91	0.98	AMR	—	—	—	0.51	>0.99	0.85
Fecundity	—	—	—	—	0.44	0.70	Fecundity	—	—	—	—	0.92	0.21
dS	—	—	—	—	—	0.71	dS	—	—	—	—	—	0.76

Final Models (constrained, path coefficients are in fig. 2)

	Mitochondrial Protein-Coding Genes (fig. 2C)						Nuclear Protein-Coding Genes (fig. 2D)						
P values[b]	Mass	RMR	AMR	Fecundity	dS	ω	*P* values[b]	Mass	RMR	AMR	Fecundity	dS	ω
Mass	—	0.03	*	0.01	*	<0.01	Mass	—	0.04	0.02	0.03	*	*
RMR	—	—	0.04	*	*	*	RMR	—	—	<0.01	*	*	*
AMR	—	—	—	*	0.02	<0.01	AMR	—	—	—	*	<0.01	<0.01
Fecundity	—	—	—	—	*	*	Fecundity	—	—	—	—	<0.01	*
dS	—	—	—	—	—	*	dS	—	—	—	—	—	*

NOTE.—R_i^2 is the variance explained by the dependent variables in the initial model.

[a] Posterior probabilities (PP) of the covariance sign: PP < 0.025 (significant negative) and PP > 0.975 (significant positive).

[b] *P* values of path coefficients of the final path model. Asterisk indicates paths that were constrained to be zero in the final model.

of connecting paths between variables implies no hypothesized direct effect.

Indirect effects between two variables are inferred by the presence of intermediate variables along the flow of a path. For example in figure 2*B*, body mass has an indirect effect on absolute rates of nuclear genes through two path flows. The first path is through the relationship of mass ↔ AMR → nuclear with an indirect effect equal to the mathematical product of the coefficients along the path flow (i.e., $-0.38 \times 0.40 = -0.152$). The second path is through the relationship of mass ↔ RMR ↔ AMR → nuclear with indirect effect equal to $-0.37 \times 0.42 \times 0.40 = -0.062$. The total effect is the sum of all direct and indirect effects between these two variables. In this case, the total effect of body mass on absolute rates of nuclear genes is $-0.152 + (-0.062) = -0.214$.

Each path coefficient also provides an idea of the consistency (i.e., reliability) of the predictor to estimate the dependent variable. The reliability is estimated by the square value of the path coefficient (e.g., the reliability of AMR for predicting the absolute rates of nuclear genes is $0.40 \times 0.40 = 0.16$). Values of reliability above >0.50 are considered to support standalone predictors (Santos and Cannatella 2011). The total variance explained by the entire model about each endogenous variable is expressed by its R^2 (e.g., 0.16 for the absolute rates of nuclear genes). The overall usefulness of the model should be evaluated by a combination of its χ^2 magnitude and significance, model fit indices (i.e., CFI, RMSEA, TLI, and SRMR), and total variance explained (R^2) of each endogenous variable.

Evidence of Higher Rates of Molecular Evolution Using Path Analysis

Several models were used to test the association between life history predictors and absolute rates, dS rates, and ω of mitochondrial and nuclear genes. The final models (fig. 2*A*–*D* and bottom of tables 3 and 4) were those with the best overall fit to the observed data. Figure 2*A* shows

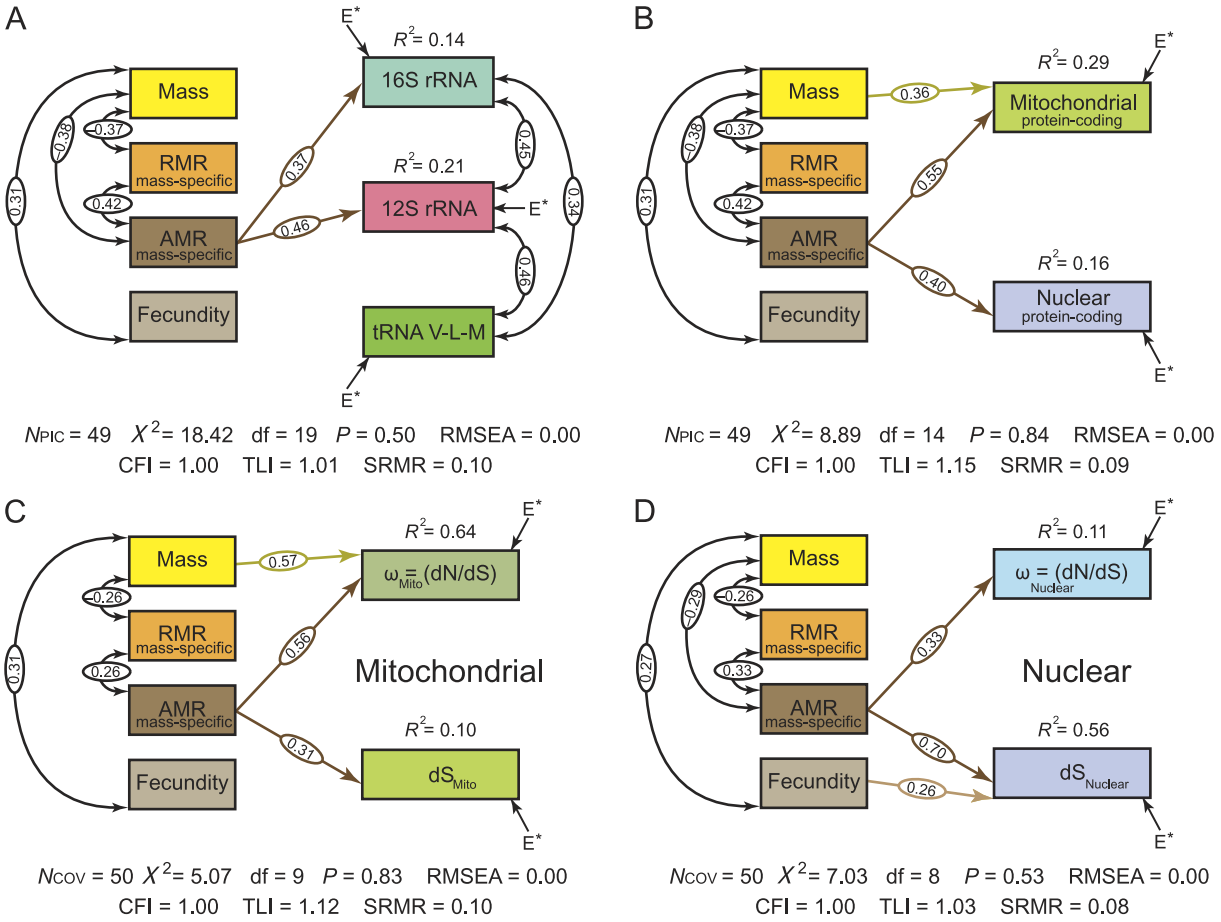

FIG. 2. Phylogenetic path analyses representing network models of life history traits, absolute rates, ω (dN/dS), and dS rates in poison frogs. (*A*) Model of life history traits (predictors-exogenous variables) as codependents on absolute rates of RNA-coding mitochondrial genes (dependents-endogenous variables); (*B*) model of life history traits as codependents on absolute rates of concatenated protein-coding mitochondrial and nuclear genes; two models of life history traits as codependents on (*C*) ω and dS rate of concatenated protein-coding mitochondrial genes and on (*D*) ω and dS rate of concatenated protein-coding nuclear genes. Connecting lines are path coefficients of causal-direct association (single-headed arrows) and correlations/covariances (double-headed arrows). The absence of connecting lines between variables implies no hypothesized direct effect. Standard path coefficients between variables are contained within ellipses. Direct effects are represented by connecting arrows between variables (e.g., AMR → 12S rRNA). Indirect effects are compound pathways that connect two variables through an intermediate variable (e.g., body mass has an indirect effect on $dS_{nuclear}$ through three ways: mass ↔ RMR ↔ AMR → $dS_{nuclear}$, mass ↔ AMR → $dS_{nuclear}$, and mass ↔ fecundity → $dS_{nuclear}$). Error variables of endogenous variables represent measurement error and unaccounted effects by unmeasured agents (e.g., life span and generation time). All error variables are significant ($P < 0.05$) and are indicated by *E**. The total variance of the endogenous variables explained by the model is summarized in the R^2. Path model statistics include χ^2 goodness of fit, Bentler's CFI > 0.95 = good fit, TLI > 0.95 = good fit, RMSEA < 0.05 = good fit, and SRMR < 0.10 = adequate fit.

the model between life history traits and RNA-coding mitochondrial genes. AMR had a direct effect on the absolute rates of 12S and 16S rRNAs, whereas body mass, RMR, and fecundity had indirect effects through AMR. None of the life history variables analyzed has a direct path to tRNAs. Although the path model fit the observed data, the explained variances of the absolute rates of 12S and 16S rDNA were low (i.e., $0.10 < R^2 < 0.30$). Figure 2*B* shows the model between life history traits on absolute rates of concatenated mitochondrial and nuclear protein-coding genes. AMR had a direct effect on absolute rates of both mitochondrial and nuclear loci, whereas body mass had a direct effect only on the rate of mitochondrial genes. RMR and fecundity had an indirect effect on absolute rates through AMR and body mass. Although the path model fit the observed data, the explained variances of mitochondrial and nuclear loci were low (i.e., $0.10 < R^2 < 0.30$). Figure 2*C* shows the model between life history traits and mitochondrial dS (dS_{Mito}) rate and ω (ω_{Mito}). AMR had a direct effect on both dS_{Mito} rate and ω_{Mito}, whereas body mass only had a direct effect on ω_{Mito}. RMR and fecundity had indirect effects on both dependents through AMR and body mass. The path model fit the observed data, and the explained variance of ω_{Mito} was acceptable (i.e., $0.30 < R^2 < 0.75$); in contrast, the explained variance of dS_{Mito} was low (i.e., $0.10 < R^2 < 0.30$). Finally, figure 2*D* shows the model between life history traits and nuclear dS ($dS_{nuclear}$) rate and ω ($\omega_{nuclear}$). AMR had a direct effect on both $dS_{nuclear}$ rate and $\omega_{nuclear}$, whereas fecundity only had a direct effect on $dS_{nuclear}$.

Body mass and RMR had indirect effects on both dependents through AMR and fecundity. The path model fit the observed data, and the explained variance of $\omega_{nuclear}$ was low (i.e., $0.10 < R^2 < 0.30$); in contrast, the explained variance of $dS_{nuclear}$ was acceptable (i.e., $0.30 < R^2 < 0.75$). Therefore, AMR was the only consistent direct predictor of rates of molecular evolution in poison frogs for both mitochondrial and nuclear loci. Body mass and fecundity were weaker direct predictors of rates of molecular evolution, and they were genome specific (i.e., body mass for mitochondrial loci and fecundity for nuclear loci). RMR was an indirect predictor of rates of molecular evolution through AMR, fecundity, or body mass.

Discussion

The balance between mutation rate, DNA repair, and replication errors mostly determines the dynamics of molecular evolution (Bromham 2009). A mutation rate is the speed at which sequence changes accumulate due to biochemical damage coupled with inefficient repair, DNA synthesis mistakes, or directed hypermutability (Graur and Li 2000; Pal et al. 2006; Bromham 2009). However, life history traits, such as metabolic rates, might influence the pace of molecular evolution by linking the frequency of oxidative damage to the likelihood of inheritance of molecular change (Martin and Palumbi 1993). My results support that mass-specific AMR is a consistent predictor of rates of molecular evolution of both nuclear and mitochondrial loci in poison frogs. I explored potential AMR correlates (i.e., body mass, fecundity, and RMR), but none seems to explain the AMR strong positive relationship with the rates of molecular evolution. Thus, several factors synergistically influence the rates of molecular evolution, but AMR and, to a lesser extent, fecundity and body mass are relevant for predicting the rates of molecular evolution in poison frogs.

The metabolic rate hypothesis predicts that species with low RMRs are likely to have slower rates of molecular evolution, especially in ectotherms (Martin et al. 1992; Martin 1999). However, phylogenetic comparative analyses on large ectotherm lineages (e.g., Arthropoda, Chelonia, and Mollusca) found no support for this association (Seddon et al. 1998; Caccone et al. 2004; Lanfear et al. 2007). My results were not different from previous reports and failed to support a significant direct association between RMR and the rates of molecular evolution. However, my data support an indirect association between RMR with molecular evolution through AMR, body mass, or fecundity. The implications of this indirect effect of RMR suggest that life history should be seen as a network of traits linked to the rate of molecular evolution. Moreover, few traits (e.g., AMR) are supported as dominant predictors, whereas others (e.g., fecundity and body mass) might exert a minor effect.

The AMR results showed a direct and positive association with the rates of molecular evolution as a single predictor and when used in path analyses. Several reasons support this association: 1) AMR reflects the athletic prowess or the upper bound of physical activity supported by oxidative respiration; 2) a high AMR is associated with target oxygen supply to muscles, which is linked to ROS production during or after aerobic exercise; and 3) AMRs are species specific; they cannot be approximated by body mass alone and might represent physiological adaptations to higher endurance (Bishop 1999; Weibel et al. 2004). Even though my results do not imply causation, they suggest that a strong positive association exists between high AMRs and faster molecular evolution in poison frogs. However, the AMR and rates of molecular evolution in poison frogs might be the result of synergistic associations with unmeasured life history traits.

Two possible candidates are longevity and generation time. Longevity has been shown to relate longer life spans with slower rates of molecular evolution (Nabholz et al. 2008). Species with long lives and late reproduction are expected to have effective or overactive DNA repair mechanisms, which provide a better management of free radicals (Galtier et al. 2009). Not surprisingly, longevity has been shown to negatively correlate with ROS production in both endotherms and ectotherms (Buttemer et al. 2010). Body mass positively correlates with lifespan, and it can be used as a proxy for testing the longevity hypothesis (Speakman 2005). Regarding generation time as predictor, reproduction tempo is expected to be inversely associated with substitution rates in germ line DNA due the accumulation of replication errors per unit time (Ohta 1993; Smith and Donoghue 2008; Thomas et al. 2010). Thus, higher rates of molecular evolution are expected to be associated with shorter generation times (Bromham et al. 1996). However, estimates of generation time are difficult to determine, and proxies such as developmental time, age at sexual maturity, or time to first sexual reproduction are used (Thomas et al. 2010; Bromham 2011).

In the case of poison frogs, the information about life spans is scarce, anecdotal, and mostly based on captive-risen individuals ($n = 14$, $\bar{X} = 5.7 \pm 2.6$ years, range = 3–11.5 years; see list in supplementary table 2, Supplementary Material online). From these data, only four species (i.e., *Dendrobates auratus*, *D. histrionicus*, *D. leucomelas*, and *D. pumilio*) have an acceptable level of confidence in the AnAge database (de Magalhaes and Costa 2009) to be reliable for comparative analyses. In addition, all available poison frog life spans might be biased from the increased life expectancy of captive-risen individuals (Bronikowski and Promisiow 2005). In spite of the limitations of longevity data, I tested if life span was associated with body mass, mass-specific AMR, and the rates of molecular evolution using all available accounts (i.e., $n = 14$). I found a significant ordinary least squares (OLS) correlation of 0.82 ($P < 0.01$) between lifespan and body mass, but a nonsignificant OLS correlation of 0.11 ($P = 0.71$) with mass-specific AMR. All OLS correlations with the rates of molecular evolution were nonsignificant ($P > 0.05$). In addition, I performed PGLS analyses, and all estimated λs of the correlations were negative, which made the correlations unreliable and suggest a low sample size.

Therefore, OLS correlations suggest that longevity, by its body mass proxy, might have a direct effect on rates of molecular evolution of mitochondrial protein-coding genes (fig. 2*B* and *C*). However, longevity is not associated with mass-specific AMR and is unable to explain the strong positive association between mass-specific AMR with the rates of molecular evolution. More reliable data on lifespans from natural populations are necessary to evaluate the longevity hypothesis of molecular evolution in poison frogs.

The age of sexual maturity is the best-known proxy of generation time in poison frogs (others are developmental time or time to first sexual reproduction, see supplementary table 2, Supplementary Material online). However, the information derives mostly from aposematic species of Clade D ($n = 19$, $\bar{X} = 10.5 \pm 2.5$ months, range = 5–14 months; see list on supplementary table 2, Supplementary Material online). In spite of this drawback, I also tested if the age of sexual maturity is associated with body mass, mass-specific AMR, and the rates of molecular evolution. I found a nonsignificant OLS correlation of 0.03 ($P = 0.91$) between the age of sexual maturity and body mass. Likewise, I found a nonsignificant OLS correlation of 0.24 ($P = 0.32$) between the age of sexual maturity and mass-specific AMR. All OLS correlations with the rates of molecular evolution were also nonsignificant ($P > 0.05$). In addition, I performed PGLS analyses, and all estimated λs of the correlations were negative, which made the correlations unreliable. Therefore, the age of sexual maturity might not explain the associations between AMR and molecular evolution. However, I cannot rule out that generation time has a direct effect on rates of molecular evolution in poison frogs.

Other life history traits might also explain the association between AMR and the rates of molecular evolution, including abiotic correlates and diversification rates. In the first case, variations in the rates of molecular evolution might be an expression of geographical distribution and environmental energy (Rohde 1992). Poison frogs are endemic to the Neotropics with significant altitudinal variation (i.e., from sea level up to Andean páramos at approximately 4,000 m above sea level); thus, the levels of solar radiation and environmental temperature might be important factors influencing poison frog rates of molecular evolution. To evaluate this hypothesis, poison frog lineages with distributional ranges >1,500 m.a.s.l. (e.g., species of Clade B along the Andes, such as *Hyloxalus*) and <600 m.a.s.l. (e.g., most of Clade D) should be tested for faster rates of molecular evolution. Interestingly, many lineages with high AMRs (e.g., *Dendrobates* from Clade D) are distributed in tropical rain forests (<250 m.a.s.l. with a mean warm temperature of ~25 °C); hence, environmental temperature might also play a role in the increase in the rate of evolution.

Regarding the diversification rates, some groups within the poison frogs have undergone extensive radiations since the Upper Miocene (i.e., <10 Ma) (Santos et al. 2009). For example, it could be tested if the evolution rates have increased in recently diversified clades. Two species clades of interest are the *Ameerega* (~11% or 31/285 of all the dendrobatid species with a crown age ~9 Ma) and the *D. ventrimaculatus* complex (~7.7% or 22/285 of all the species with a crown age ~7 Ma). Interestingly, both groups also concentrate many species with high AMRs, which suggests that metabolic rates might also contribute to diversification rates. More molecular data, in terms of molecular markers and taxon sampling, will be necessary to address if an association exists between AMRs, rates of diversification, and molecular evolution in poison frogs.

Aposematism is associated with AMR, RMR, Scope, and body mass in poison frogs (Santos and Cannatella 2011). As a complex phenotype in dendrobatids, aposematism is defined by the simultaneous presence of conspicuous coloration and chemical defense as skin alkaloids (Santos et al. 2003). Aposematic dendrobatids are highly polymorphic in terms of coloration, and conspicuousness is strongly associated with intraspecific (e.g., mate choice) and interspecific (e.g., Batesian and Müllerian mimicry) interactions (Summers et al. 1999; Symula et al. 2001; Darst et al. 2006). In addition to be chemically defended, poison frogs have become resistant to their own alkaloids by directional selection on key protein sites (Daly et al. 1980; Wang and Wang, 1998). For example, pumiliotoxins are targeted to muscular ion channels (e.g., Ca^{2+} and Na^{+}) causing cardiotoxic and myotoxic detrimental effects (Daly 1998; Daly et al. 1999). The physiological cost of resistance to pumiliotoxins is unknown in poison frogs, but it might be hypothesized to be higher (e.g., increased RMR or AMR) than in the susceptible nondefended species. However, the genes used in the present study (i.e., mitochondrial and nuclear) are not related to aposematism and are expected to be under strong negative selection. Further analyses at the genomic level might determine if aposematic genes related to high AMR are undergoing positive selection and have faster rates of molecular evolution.

Aerobic Exercise Link: AMR, Oxygen Supply, ROS Production, and Rates of Molecular Evolution

AMR is determined by the maximal oxygen consumption ($\hat{V}_{O_2max}$), where mitochondrial efficiency is near its highest capacity to consume oxygen (Gatten et al. 1992; Wagner 2008). Variations in AMRs primarily derive from specific adaptations to endure physical activity (Wagner 2008) and less likely from mitochondrial efficiency (Roca et al. 1989; Gonzalez et al. 2006). Specifically, the evolution of AMR should be mostly reflected in adaptations for systemic oxygen transportation (Weibel 1984; Hillman et al. 2009) such as lung capacity for air ventilation, oxygen diffusion from alveolar gas to transporting proteins in the blood, targeted blood flow to active muscles during exercise by the cardiovascular system, and oxygen diffusion to mitochondria to achieve their near $\hat{V}_{O_2max}$ capacity.

AMR and athletic prowess are related by how fast oxygen is supplied by the cardiopulmonary system to skeletal muscles (Bishop 1999) and the total volume of mitochondria (Weibel and Hoppeler 2005). For example, well-trained individuals (e.g., human athletes and active endotherm

predators) have a higher aerobic capacity reflected by an efficient oxygen supply to muscles during activity, which rises $\hat{V}_{O_2max}$ to near the asymptotic maximum $\hat{V}_{O_2}$ seen in isolated mitochondria (Gonzalez et al. 2006; Wagner 2008). The increased oxygen intake during physical activity promotes the production of free radicals, such as ROS, in several orders of magnitude (Tonkonogi et al. 2000; Di Meo and Venditti 2001; Powers and Jackson 2008). ROS excess production is known to be associated with bursts of oxidative stress, which then is coupled with senescence and higher mutation rates (Galtier et al. 2009). Therefore, higher AMRs and faster rates of molecular evolution should be positively correlated if exercise-related ROS and oxidative stress are not managed with efficient antioxidant enzymes (e.g., hyperactive superoxide dismutase).

The magnitude of the association between AMR and substitution rates varied among the analyzed loci. For instance, in the mitochondrial genome, AMR was positively associated with absolute rates of RNA-coding mitochondrial genes (i.e., 12S and 16S rDNAs), which might reflect higher substitution rates in fast evolving sequence motifs (e.g., RNA loops) (Kjer 1995; Hickson et al. 1996). Likewise, AMR was positively associated with absolute rates of protein-coding genes, which suggest an increase on mutation rates due to oxidative damage and a weaker effect of selection. In contrast, AMR was not associated with the rates of tRNAs, which is unexpected if higher AMR causes a general increase in mutation rates. This discrepancy could be explained by the fact that the three tRNAs used do not have enough information (i.e., tRNAs V–L–M has 221 bp vs. ~5,000 bp of the nuclear loci). In addition, mitochondrial tRNAs have their stem–loop structure conserved (Pesole et al. 1999), and entire mitochondrial genomes might be necessary to determine if AMRs are associated with rates of molecular evolution of tRNAs. Overall, substitution rates in mitochondria are dependent on the quantity of ROS produced during physical exercise, the DNA repair efficiency, and the strength of the purifying selection upon the analyzed loci (Yakes and VanHouten 1997; Hirsh and Fraser 2001; Meiklejohn et al. 2007).

The interpretation of the direct relationship between AMR and molecular evolution in nuclear genes is challenging. Based on our current knowledge, mitochondria produce free radicals that represent 1–4% of all the oxygen respired by air-breathing organisms (Yu 2005). The ROS produced by mitochondria represent 80–90% of all superoxides produced, but the remaining 10–20% originates from several sources widely distributed throughout the cell (Balaban et al. 2005). In mammals, mitochondrial ROS appears to have a negligible contribution to the oxidative damage observed in nuclear DNA (Hoffmann et al. 2004; Michaelson et al. 2010). Moreover, a high aerobic metabolism appears to be independent or drives a slightly negative effect on DNA mutation rates in mice and rats (Tweedie et al. 2011). However, constant oxidative DNA damage has been evidenced regardless of the ROS production by mitochondria (Hoffmann et al. 2004).

In spite of the mitochondrial ROS constraint, cytosolic endogenous ROS causes nuclear oxidative DNA damage and genetic instability (Chen et al. 1995). Intracellular nonmitochondrial ROS might originate from several sources (e.g., membrane-associated oxidases, lipoxygenases, and cythochromes) (Yu 2005), including enzymes related to muscle contraction (Michaelson et al. 2010). Likewise, extracellular agents of oxidative stress might increase the ROS production such as light radiation (Hoffmann et al. 2004), hypoxia (Chandel et al. 1998), hyperoxia (Fehrenbach and Northoff 2001), and toxins (Azqueta et al. 2009). Additional evidence suggests that different levels of ROS damage exist between active tissues (e.g., type I skeletal muscles) and more passive cell types within a single organism (Amara et al. 2007; Powers et al. 2011). Overall, high AMR and faster rates of molecular evolution are possible on remote and less metabolically active germ line cells by nonmitochondrial ROS. Much experimental information needs to be collected on ROS nonmitochondrial sources and extracellular inductors of DNA damage.

One significant parameter related to AMR is the efficiency of oxygen supply to active tissues by the cardiovascular system (Bishop 1999; Di Meo and Venditti 2001; Fehrenbach and Northoff 2001). During physical activity, such as active predation, the supply of oxygen is targeted to skeletal muscles and decreases towards less active tissues (e.g., liver and germ line cells) by reduced blood flow (Di Meo and Venditti 2001; Bickler and Buck 2007). By assuming that mitochondrial aerobic respiration is limited by the supply of oxygen, less active tissues, such as germ line cells, might experience periodic reductions of oxygen supply (i.e., partial ischemia or hypoxia) related to aerobic exercise. Alternatively, after the exercise has ended, the resting state is preceded by an increase in blood flow (i.e., reoxygenation) by the cardiovascular system to the ischemic tissues, which could potentiate the production of ROS in germ cells by hyperoxia (Bickler and Buck 2007). Therefore, as a byproduct of exercise hyperoxia or hypoxia, high AMR species might experience frequent peaks of ROS production that increases DNA damage and mutation in less active tissues such as germ cells.

AMR reflects the species-specific capacity to perform aerobic exercise. Interestingly, at the intraspecific level, exercise-induced hyperoxia or hypoxia has been evidenced to induce oxidative stress, senescence, and DNA damage across taxa including flies (Agarwal and Sohal 1994; Rascon and Harrison 2010), fish (Lushchak et al. 2005; Bickler and Buck 2007), amphibians (Bickler and Buck 2007), reptiles (Bickler and Buck 2007), and endotherms (Vonzglinicki et al. 1995; Moller et al. 2001). These evidences suggest that AMR positively correlates with ROS production during exercise across ectotherm and endotherm lineages. Furthermore, AMR, as a proxy of ROS production, might positively correlate with DNA damage and rates of molecular evolution at both nuclear and mitochondrial loci. Future work is needed to test the generality of the AMR mechanistic hypothesis.

The mechanistic link between AMR and rates of molecular evolution can be summarized as follows: 1) AMR is

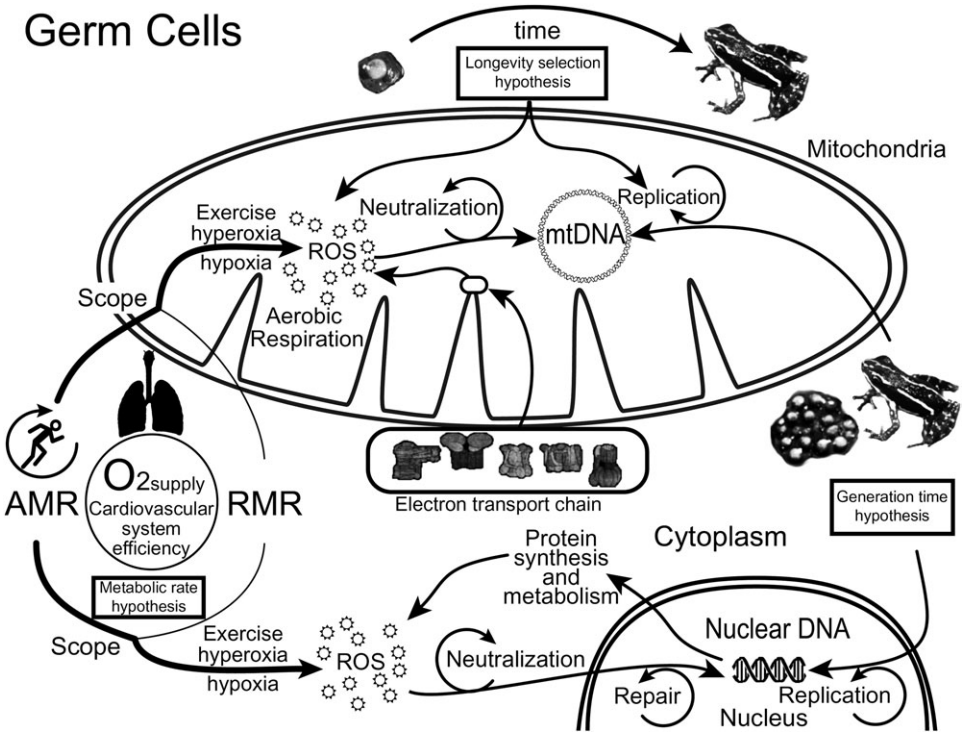

Fig. 3. Summary of the three hypotheses of molecular evolution with their causal associations in poison frogs. The metabolic rate hypothesis considers the production of ROS in relation with resting (RMR), nonsustainable physical activity (AMR), and Scope (difference between AMR and RMR). The generation time hypothesis refers to the pace of DNA synthesis in the germ line per unit time. The longevity hypothesis is related to the efficiency of DNA replication, mutation repair, time of reproduction, and management of oxidative stress (e.g., reduction of ROS production). The results of the comparative analyses support a multifactorial model including AMR as a significant predictor of the rates of molecular evolution for both mitochondrial and nuclear loci.

a measurement of the aerobic capacity and oxygen supply by the cardiovascular system to the active tissues during aerobic exercise; 2) mitochondrial efficiency is not related to AMR because mitochondria are near their maximum capacities to consume oxygen (V_{O2max}) and limited only by oxygen supply; 3) target blood flow to active muscles promotes partial ischemia (i.e., hypoxia or reduced oxygen supply) to less active tissues such as germ line cells; 4) after exercise has ended, reoxygenation to ischemic tissues (e.g., germ line cells) might cause hyperoxia (i.e., excess of oxygen) by increased blood flow; 5) both hyperoxia and hypoxia are well-known physiological causes of ROS production and DNA damage; 6) AMR, by proxy, also measures ROS production during exercise in the whole organism including germ line cells; 7) high ROS levels are well-known causes faster rates of molecular evolution if mechanisms that control ROS production are less efficient or absent; and 8) high AMR species might experience more frequent burst of exercise-related oxidative damage and faster rates of molecular evolution.

Multifactorial Model of Molecular Evolution Including AMR

Three main hypotheses explain the variability in rates of molecular evolution among lineages and genomes, namely, generation time, longevity, and metabolic rate hypotheses (fig. 3). The current perception is that molecular evolution is a synergistic result of many direct and indirect life history agents whose main correlate is body size (Bromham 2011). To my knowledge, my results are the first to support an addition factor related to aerobic capacity in the form of AMR or Scope, which affects the rate of molecular evolution in ectotherms.

Multivariate approaches, such as path analysis, are more suitable for addressing casual–correlative structures of molecular evolution and life history traits. All the estimated models are driven by AMRs for the following reasons: 1) AMR is a better estimate of the potential generation of ROS free radicals than RMR (Schmidt-Nielsen 1984); 2) AMR is closer to the actual energetic cost under natural conditions and closer to the FMR or the average daily metabolic rate (Gatten et al. 1992); 3) AMR is species-specific and reflects the athletic prowess, which is a better predictor of ROS production during aerobic exercise (Tonkonogi et al. 2000); 5) the increased ROS production due to hyperoxia or hypoxia related to differential oxygen supply during physical activity might significantly contribute to oxidative stress, DNA damage, and rates of molecular evolution in both nuclear and mitochondrial loci; and 6) single predictor or multivariate models consistently support AMR to be associated with rates of molecular evolution. Therefore, the assessments of molecular evolution might need to be expanded to include AMR or its metabolic proxies (e.g., Scope).

A multifactorial model based on AMR has the following assumptions: 1) the oxygen intake during physical activity is coupled with the production of oxidative free radicals (e.g., ROS); 2) the cellular respiration during physical activity is associated with mitochondrial DNA damage; 3) extramitochondrial ROS produced during physical activity causes oxidative damage to nuclear DNA and genetic instability; 4) AMR reflects the ROS generation level induced on germ cells by differential oxygen supply during or after aerobic exercise; 5) the mutation rates of both nuclear and mitochondrial genomes are directly associated with ROS production; and 6) variations in molecular evolution is a multifactorial outcome related to DNA repair, extracellular mutagens, generation time, lifespan, and other genomic idiosyncrasies (e.g., organellar vs. nuclear). In the case of poison frogs, other factors (e.g., aposematism, diversification rates, and climatic variables) might be relevant factors affecting the rates of molecular evolution, and they should be further studied.

A likely expectation of the direct effect of AMR on rates of molecular evolution is a molecular clock similar to the RMR-based metabolic hypothesis (Martin and Palumbi 1993; Kumar and Hedges 1998). Additional data on sequences under neutral or near neutral evolution (e.g., introns and pseudogenes) should be analyzed to understand the implications of the association between AMR and rates of molecular evolution. The observed path models reflect the need of network-like descriptions of the interactions between life history traits and molecular evolution. Finally, the evolution at molecular level should be considered as a multifactor outcome (Cortopassi and Wang 1996; Williams 1996; Perez-Campo et al. 1998), and phylogenetic path analyses might provide testable models of molecular evolution.

Supplementary Materials

Supplementary figure 1 and tables 1–8 are available at *Molecular Biology and Evolution* online (http://www.mbe.oxfordjournals.org/).

Acknowledgments

J.C.S. thanks David Cannatella for his support during his PhD studies. J.C.S. thanks B. Redelings, N. Lartillot, and R. Lanfear for their help in the analyses. N. Biani and I. Santos have been a source of kindness and support. J.C.S. thanks anonymous reviewers for their suggestions. Collection permits were provided by specific institutions from Panamá (SE/A-4-6), Ecuador (0004-IC-FAU-DNBAP/MA, 0006-IC-FAU-DNBAP/MA, 016-IC-FAU-DNBAP/MA, 027-IC-FAU-DNBAPVS/MA), and Venezuela (Decreto N°5125 to C. Barrio). The University of Texas Ecology, Evolution, and Behavior fellowships to J.C.S. and National Science Foundation (NSF) grants to David Cannatella (DDIG DEB-0710033 and EF-0334952) provided financial support for this research. J.C.S. was also supported by the National Evolutionary Synthesis Center (NSF grants EF-0423641 and EF-0905606).

References

Agarwal S, Sohal RS. 1994. DNA oxidative damage and life expectancy in houseflies. *Proc Natl Acad Sci U S A.* 91:12332–12335.

Alwin DF, Hauser RM. 1975. The decomposition of effects in path analysis. *Am Sociol Rev.* 40:37–47.

Amara CE, Shankland EG, Jubrias SA, Marcinek DJ, Kushmerick MJ, Conley KE. 2007. Mild mitochondrial uncoupling impacts cellular aging in human muscles in vivo. *Proc Natl Acad Sci U S A.* 104:1057–1062.

Azqueta A, Shaposhnikov S, Collins AR. 2009. DNA oxidation: investigating its key role in environmental mutagenesis with the comet assay. *Mutat Res.* 674:101–108.

Balaban RS, Nemoto S, Finkel T. 2005. Mitochondria, oxidants, and aging. *Cell* 120:483–495.

Benjamini Y, Hochberg Y. 1995. Controlling the false discovery rate—a practical and powerful approach to multiple testing. *J R Stat Soc Ser B Methodol.* 57:289–300.

Bentler PM. 1990. Comparative fit indexes in structural models. *Psychol Bull.* 107:238–246.

Bentler PM. 1995. EQS structural equations program manual. Encino (CA): Multivariate Software.

Bickler PE, Buck LT. 2007. Hypoxia tolerance in reptiles, amphibians, and fishes: life with variable oxygen availability. *Annu Rev Physiol.* 69:145–170.

Bishop CM. 1999. The maximum oxygen consumption and aerobic scope of birds and mammals: getting to the heart of the matter. *Proc R Soc Lond B Biol Sci.* 266:2275–2281.

Bromham L. 2009. Why do species vary in their rate of molecular evolution? *Biol Lett.* 5:401–404.

Bromham L. 2011. The genome as a life-history character: why rate of molecular evolution varies between mammal species. *Philos Trans R Soc Lond B Biol Sci.* 366:2503–2513.

Bromham L, Penny D. 2003. The modern molecular clock. *Nat Rev Genet.* 4:216–224.

Bromham L, Penny D, Rambaut A, Hendy MD. 2000. The power of relative rates tests depends on the data. *J Mol Evol.* 50:296–301.

Bromham L, Rambaut A, Harvey PH. 1996. Determinants of rate variation in mammalian DNA sequence evolution. *J Mol Evol.* 43:610–621.

Bronikowski AM, Promisiow DEL. 2005. Testing evolutionary theories of aging in wild populations. *Trends Ecol Evol.* 20: 271–273.

Brown JH, Gillooly JF, Allen AP, Savage VM, West GB. 2004. Toward a metabolic theory of ecology. *Ecology* 85:1771–1789.

Brown JH, West GB, Enquist BJ. 2000. Scaling in Biology: patterns, processes, causes, and consequences. In: Brown JH, West GB, editors. Scaling in biology. New York: Oxford University Press. p. 1–24.

Brown JM, Pauly GB. 2005. Increased rates of molecular evolution in an equatorial plant clade: an effect of environment or phylogenetic nonindependence? *Evolution* 59:238–242.

Browne MW, Cudeck R. 1993. Alternative ways of assessing model fit. In: Bollen KA, Long JS, editors. Testing structural equation models. Beverly Hills (CA): Sage Publications. p. 136–162.

Butler PJ, Green JA, Boyd IL, Speakman JR. 2004. Measuring metabolic rate in the field: the pros and cons of the doubly labelled water and heart rate methods. *Funct Ecol.* 18:168–183.

Buttemer WA, Abele D, Costantini D. 2010. From bivalves to birds: oxidative stress and longevity. *Funct Ecol.* 24:971–983.

Caccone A, Gentile G, Burns CE, Sezzi E, Bergman W, Ruelle M, Saltonstall K, Powell JR. 2004. Extreme difference in rate of mitochondrial and nuclear DNA evolution in a large ectotherm, Galapagos tortoises. *Mol Phylogenet Evol.* 31:794–798.

Chandel NS, Maltepe E, Goldwasser E, Mathieu CE, Simon MC, Schumacker PT. 1998. Mitochondrial reactive oxygen species

trigger hypoxia-induced transcription. *Proc Natl Acad Sci U S A.* 95:11715–11720.
Chen Q, Fischer A, Reagan JD, Yan LJ, Ames BN. 1995. Oxidative dna-damage and senescence of human-diploid fibroblast cells. *Proc Natl Acad Sci U S A.* 92:4337–4341.
Cortopassi GA, Wang E. 1996. There is substantial agreement among interspecies estimates of DNA repair activity. *Mech Ageing Dev.* 91:211–218.
Daly JW. 1998. Thirty years of discovering arthropod alkaloids in amphibian skin. *J Nat Prod* 61:162–172.
Daly JW, Garraffo HM, Spande TF. 1999. Alkaloids from amphibian skins. In: Pelletier SW, editor. Alkaloids: chemical and biological perspectives. New York: Pergamon Press. p. 1–161.
Daly JW, Myers CW, Warnick JE, Albuquerque EX. 1980. Levels of batrachotoxin and lack of sensitivity to its action in poison-dart frogs (*Phyllobates*). *Science* 208:1383–1385.
Darst CR, Cummings ME, Cannatella DC. 2006. A mechanism for diversity in warning signals: conspicuousness versus toxicity in poison frogs. *Proc Natl Acad Sci U S A.* 103:58252–155857.
de Magalhaes JP, Costa J. 2009. A database of vertebrate longevity records and their relation to other life-history traits. *J Evol Biol.* 22:1770–1774.
Di Meo S, Venditti P. 2001. Mitochondria in exercise-induced oxidative stress. *Biol Signals Recept.* 10:125–140.
Drummond AJ, Rambaut A. 2007. BEAST: Bayesian evolutionary analysis by sampling trees. *BMC Evol Biol.* 7:214.
Fehrenbach E, Northoff H. 2001. Free radicals, exercise, apoptosis, and heat shock proteins. *Exerc Immunol Rev.* 7:66–89.
Felsenstein J. 1985. Phylogenies and the comparative method. *Am Nat.* 125:1–15.
Foksinski M, Rozalski R, Guz J, Ruszkowska B, Sztukowska P, Piwowarski M, Klungland A, Olinski R. 2004. Urinary excretion of DNA repair products correlates with metabolic rates as well as with maximum life spans of different mammalian species. *Free Radic Biol Med.* 37:1449–1454.
Galtier N, Jobson RW, Nabholz B, Glemin S, Blier PU. 2009. Mitochondrial whims: metabolic rate, longevity and the rate of molecular evolution. *Biol Lett.* 5:413–416.
Garland T. 1992. Rate tests for phenotypic evolution using phylogenetically independent contrasts. *Am Nat.* 140:509–519.
Garland T, Harvey PH, Ives AR. 1992. Procedures for the analysis of comparative data using phylogenetically independent contrasts. *Syst Biol.* 41:18–32.
Garland T, Ives AR. 2000. Using the past to predict the present: confidence intervals for regression equations in phylogenetic comparative methods. *Am Nat.* 155:346–364.
Gatten RE, Miller KJ, Full RJ. 1992. Energetics at rest and during locomotion. In: Feder ME, Burggren WW, editors. Environmental physiology of the amphibians. Chicago (IL): The University of Chicago. p. 314–377.
Gillooly JF, Allen AP, West GB, Brown JH. 2005. The rate of DNA evolution: effects of body size and temperature on the molecular clock. *Proc Natl Acad Sci U S A* 102:140–145.
Gonzalez NC, Kirkton SD, Howlett RA, Britton SL, Koch LG, Wagner HE, Wagner PD. 2006. Continued divergence in Vo2max of rats artificially selected for running endurance is mediated by greater convective blood O-2 delivery. *J Appl Physiol.* 101:1288–1296.
Grace JB. 2006. Structural equation modeling and natural systems. Cambridge: Cambridge University Press.
Graur D, Li WH. 2000. Fundamentals of molecular evolution. Sunderland (MA): Sinauer Associates.
Hamilton MB. 2009. Population genetics. Oxford: Wiley-Blackwell.
Harmon LJ, Weir JT, Brock CD, Glor RE, Challenger W. 2008. GEIGER: investigating evolutionary radiations. *Bioinformatics* 24:129–131.
Hickson RE, Simon C, Cooper A, Spicer GS, Sullivan J, Penny D. 1996. Conserved sequence motifs, alignments, and secondary structure for the third domain of animal 12S rRNA. *Mol Biol Evol.* 13:150–169.
Hillman SS, Withers PC, Drewes RC, Hillyard SD. 2009. Ecological and environmental physiology of amphibians. Oxford: Oxford University Press.
Hirsh AE, Fraser HB. 2001. Protein dispensability and rate of evolution. *Nature* 411:1046–1049.
Hoeeg S, Vences M, Brinkmann H, Meyer A. 2004. Phylogeny and comparative substitution rates of frogs inferred from sequences of three nuclear genes. *Mol Biol Evol.* 21:1188–1200.
Hoffmann S, Spitkovsky D, Radicella JP, Epe B, Wiesner RJ. 2004. Reactive oxygen species derived from the mitochondrial respiratory chain are not responsible for the basal levels of oxidative base modifications observed in nuclear DNA of mammalian cells. *Free Radic Biol Med.* 36:765–773.
Hu L, Bentler PM. 1999. Cutoff criteria for fit indexes in covariance structure analysis: conventional criteria versus new alternatives. *Struct Equ Modeling.* 6:1–55.
Huelsenbeck JP, Ronquist FP. 2001. MRBAYES: Bayesian inference of phylogenetic trees. *Bioinformatics* 17:754–755.
Karasov WH, Martinez del Rio C. 2007. Physiological ecology: how animals process energy, nutrients, and toxins. Princeton (NJ): Princeton University Press.
Kjer KM. 1995. Use of rRNA secondary structure in phylogenetic studies to identify homologous positions: an example of alignment and data presentation from the frogs. *Mol Phylogenet Evol.* 4:314–330.
Kline R. 2005. Pinciples and practice of structural equation modeling. New York: Guilford Press.
Kumar S, Hedges SB. 1998. A molecular timescale for vertebrate evolution. *Nature* 392:917–920.
Lanfear R, Thomas JA, Welch JJ, Brey T, Bromham L. 2007. Metabolic rate does not calibrate the molecular clock. *Proc Natl Acad Sci U S A.* 104:15388–15393.
Lanfear R, Welch JJ, Bromham L. 2010. Watching the clock: studying variation in rates of molecular evolution between species. *Trends Ecol Evol.* 25:495–503.
Lartillot N, Lepage T, Blanquart S. 2009. PhyloBayes 3: a Bayesian software package for phylogenetic reconstruction and molecular dating. *Bioinformatics* 25:2286–2288.
Lartillot N, Poujol R. 2011. A phylogenetic model for investigating correlated evolution of substitution rates and continuous phenotypic characters. *Mol Biol Evol.* 28:729–744.
Lemmon AR, Moriarty EC. 2004. The importance of proper model assumption in Bayesian phylogenetics. *Syst Biol.* 53:265–277.
Lushchak VI, Bagnyukova TV, Husak VV, Luzhna LI, Lushchak OV, Storey KB. 2005. Hyperoxia results in transient oxidative stress and an adaptive response by antioxidant enzymes in goldfish tissues. *Int J Biochem Cell Biol.* 37:1670–1680.
Martin AP. 1999. Substitution rates of organelle and nuclear genes in sharks: implicating metabolic rate (again). *Mol Biol Evol.* 16: 996–1002.
Martin AP, Naylor GJP, Palumbi SR. 1992. Rates of mitochondrial-dna evolution in sharks are slow compared with mammals. *Nature* 357:153–155.
Martin AP, Palumbi SR. 1993. Body size, metabolic rate, generation time, and the molecular clock. *Proc Natl Acad Sci U S A.* 90: 4087–4091.
Martins E, Hansen TF. 1997. Phylogenies and the comparative method: a general approach to incorporating phylogenetic information into the analysis of interspecific data. *Am Nat.* 149:646–667.
Meiklejohn CD, Montooth KL, Rand DM. 2007. Positive and negative selection on the mitochondrial genome. *Trends Genet.* 23:259–263.

Michaelson LP, Shi GL, Ward CW, Rodney GG. 2010. Mitochondrial redox potential during contraction in single intact muscle fibers. *Muscle Nerve* 42:522–529.
Moller P, Loft S, Lundby C, Olsen NV. 2001. Acute hypoxia and hypoxic exercise induce DNA strand breaks and oxidative DNA damage in humans. *FASEB J.* 15:1181–1186.
Monaghan P, Metcalfe NB, Torres R. 2009. Oxidative stress as a mediator of life history trade-offs: mechanisms, measurements and interpretation. *Ecol Lett.* 12:75–92.
Muthén BO, Muthén LK. 2011. Mplus (statistical analysis with latent variables). Los Angeles (CA): Muthén & Muthén.
Nabholz B, Glémin S, Galtier N. 2008. Strong variations of mitochondrial mutation rate across mammals—the longevity hypothesis. *Mol Biol Evol.* 25:120–130.
Nagy KA. 2005. Field metabolic rate and body size. *J Exp Biol.* 208:1621–1625.
Ohta T. 1993. An examination of the generation-time effect on molecular evolution. *Proc Natl Acad Sci U S A.* 90:10676–10680.
Pagel M. 1993. Seeking the evolutionary regression coefficient: an analysis of what comparative methods measure. *J Theor Biol.* 164:191–205.
Pagel M. 1997. Inferring evolutionary processes from phylogenies. *Zool Scr.* 26:331–348.
Pagel M. 1999. Inferring the historical patterns of biological evolution. *Nature* 401:877–884.
Pal C, Papp B, Lercher MJ. 2006. An integrated view of protein evolution. *Nat Rev Genet.* 7:337–348.
Paradis E, Claude J, Strimmer K. 2004. APE: analyses of phylogenetics and evolution in R language. *Bioinformatics* 20:289–290.
Perez-Campo R, Lopez-Torres M, Cadenas S, Rojas C, Barja G. 1998. The rate of free radical production as a determinant of the rate of aging: evidence from the comparative approach. *J Comp Physiol B.* 168:149–158.
Pesole G, Gissi C, De Chirico A, Saccone C. 1999. Nucleotide substitution rate of mammalian mitochondrial genomes. *J Mol Evol.* 48:427–434.
Pinheiro J, Bates D, DebRoy S, Sarkar D, R-Core Team. 2011. nlme: linear and nonlinear mixed effects models [Internet]. R package. Version 3.1-102 [cited 2011 Jul 29]. Available from: http://cran.r-project.org/web/packages/nlme/index.html
Posada D, Buckley TR. 2004. Model selection and model averaging in phylogenetics: advantages of the AIC and Bayesian approaches over likelihood ratio tests. *Syst Biol.* 53:793–808.
Posada D, Crandall KA. 1998. Modeltest: testing the model of DNA substitution. *Bioinformatics* 14:817–818.
Powers SK, Jackson MJ. 2008. Exercise-induced oxidative stress: cellular mechanisms and impact on muscle force production. *Physiol Rev.* 88:1243–1276.
Powers SK, Nelson WB, Hudson MB. 2011. Exercise-induced oxidative stress in humans: cause and consequences. *Free Radic Biol Med.* 51:942–950.
Rambaut A. 2009. FigTree: tree figure drawing tool [Internet]. Edinburgh (UK) [cited 2011 Jan 20]. Available from: http://tree.bio.ed.ac.uk/software/figtree/
Rambaut A, Charleston MA. 2002. TreeEdit: phylogenetic tree [Internet]. Oxford [cited 2011 Jul 29]. Available from: http://tree.bio.ed.ac.uk/software/treeedit/
Rambaut A, Drummond AJ. 2007. Tracer v1.4 [Internet]. [cited 2011 Jul 29]. Available from: http://beast.bio.ed.ac.uk/Tracer
Rand DM. 1994. Thermal habit, metabolic-rate and the evolution of mitochondrial-dna. *Trends Ecol Evol.* 9:125–131.
Rascon B, Harrison JF. 2010. Lifespan and oxidative stress show a non-linear response to atmospheric oxygen in Drosophila. *J Exp Biol.* 213:3441–3448.
Ricklefs RE. 2008. The evolution of senescence from a comparative perspective. *Funct Ecol.* 22:379–392.
Roca J, Hogan MC, Story D, Bebout DE, Haab P, Gonzalez R, Ueno O, Wagner PD. 1989. Evidence for tissue diffusion limitation of VO2max in normal humans. *J Appl Physiol.* 67:291–299.
Rohde K. 1992. Latitudinal gradients in species diversity: the search for the primary cause. *Oikos* 65:514–527.
Rohlf FJ. 2001. Comparative methods for the analysis of continuous variables: geometric interpretations. *Evolution* 55:2143–2160.
Sanderson MJ. 2002. Estimating absolute rates of molecular evolution and divergence times: a penalized likelihood approach. *Mol Biol Evol.* 19:101–109.
Santos JC, Cannatella DC. 2011. Phenotypic integration emerges from aposematism and scale in poison frogs. *Proc Natl Acad Sci U S A.* 108:6175–6180.
Santos JC, Coloma LA, Cannatella DC. 2003. Multiple, recurring origins of aposematism and diet specialization in poison frogs. *Proc Natl Acad Sci U S A.* 100:12792–12797.
Santos JC, Coloma LA, Summers K, Caldwell JP, Ree R, Cannatella DC. 2009. Amazonian amphibian diversity is primarily derived from late Miocene Andean lineages. *PLoS Biol.* 7:e56.
Scheiner SM, Mitchell RJ, Callahan HS. 2000. Using path analysis to measure natural selection. *J Evol Biol.* 13:423–433.
Schmidt-Nielsen K. 1984. Scaling: why is animal size so important? Cambridge: Cambridge University Press.
Seddon JM, Beaverstock PR, Georges A. 1998. The rate of mitochondrial 12S rRNA gene evolution is similar in freshwater turtles and marsupials. *J Mol Evol.* 46:460–464.
Smith SA, Donoghue MJ. 2008. Rates of molecular evolution are linked to life history in flowering plants. *Science* 322:86–89.
Speakman JR. 2005. Body size, energy metabolism and lifespan. *J Exp Biol.* 208:1717–1730.
Stamatakis AR. 2006. RAxML-VI-HPC: maximum likelihood-based phylogenetic analyses with thousands of taxa and mixed models. *Bioinformatics* 22:2688–2690.
Summers K. 2000. Mating and aggressive behaviour in dendrobatid frogs from Corcovado National Park, Costa Rica: a comparative study. *Behaviour* 137:7–24.
Summers K, Symula R, Clough M, Cronin T. 1999. Visual mate choice in poison frogs. *Proc Biol Sci.* 266:2141–2145.
Swofford DL. 2000. PAUP* phylogenetic analysis using parsimony (*and other methods). Sunderland (MA): Sinauer Associates.
Symula R, Schulte R, Summers K. 2001. Molecular phylogenetic evidence for a mimetic radiation in Peruvian poison frogs supports a Mullerian mimicry hypothesis. *Proc R Soc Lond B Biol Sci.* 268:2415–2421.
Tabachnick BG, Fidell LS. 2007. Using multivariate statistics. Boston (MA): Pearson Education.
Thomas JA, Welch JJ, Lanfear R, Bromham L. 2010. A generation time effect on the rate of molecular evolution in invertebrates. *Mol Biol Evol.* 27:1173–1180.
Tonkonogi M, Walsh B, Svensson M, Sahlin K. 2000. Mitochondrial function and antioxidative defence in human muscle: effects of endurance training and oxidative stress. *J Physiol Lond.* 528:379–388.
Townsend TM, Alegre ER, Kelley ST, Wiens JJ, Reeder TW. 2008. Rapid development of multiple nuclear loci for phylogenetic analysis using genomic resources: an example from the squamate reptile. Tree of Life project. Mol Phylogenet Evol. 47:129–142
Tucker LR, Lewis C. 1973. The reliability coefficient for maximum likelihood factor analysis. *Psychometrika* 38:1–10.
Tweedie C, Romestaing C, Burelle Y, Safdar A, Tarnopolsky MA, Seadon S, Britton SL, Koch LG, Hepple RT. 2011. Lower oxidative DNA damage despite greater ROS production in muscles from rats selectively bred for high running capacity. *Am J Physiol Regul Integr Comp Physiol.* 300:R544–R553.

Vonzglinicki T, Saretzki G, Docke W, Lotze C. 1995. Mild hyperoxia shortens telomeres and inhibits proliferation of fibroblasts: a model for senescence? *Exp Cell Res.* 220:186–193.

Wagner PD. 2008. Systemic oxygen transport and utilization. *J Breath Res.* 2:doi: 10.1088/1752–7155/1082/1082/024001.

Wang SY, Wang GK. 1998. Point mutations in segment I-S6 render voltage-gated Na+ channels resistant to batrachotoxin. *Proc Natl Acad Sci U S A.* 95:2653–2658.

Weibel ERK. 1984. The pathway for oxygen. Structure and function in the mammalian respiratory system. Cambridge (MA): Harvard University Press.

Weibel ER, Bacigalupe LD, Schmitt B, Hoppeler H. 2004. Allometric scaling of maximal metabolic rate in mammals: muscle aerobic capacity as determinant factor. *Respir Physiol Neurobiol.* 140:115–132.

Weibel ER, Hoppeler H. 2005. Exercise-induced maximal metabolic rate scales with muscle aerobic capacity. *J Exp Biol.* 208:1635–1644.

Welch JJ, Bininda-Emonds ORP, Bromham L. 2008. Correlates of substitution rate variation in mammalian protein-coding sequences. *BMC Evol Biol.* 8:53.

Welch JJ, Waxman D. 2008. Calculating independent contrasts for the comparative study of substitution rates. *J Theor Biol.* 251:667–678.

Wells KD. 2007. The ecology and behavior of amphibians. Chicago (IL): University Of Chicago Press.

Williams RJP. 1996. From dihydrogen to dioxygen: evolution of biological oxidation-reduction. In: Baltscheffsky H, editor. Origin and evolution of biological energy conversion. New York: VCH Publishers. p. 109–141.

Yakes FM, VanHouten B. 1997. Mitochondrial DNA damage is more extensive and persists longer than nuclear DNA damage in human cells following oxidative stress. *Proc Natl Acad Sci U S A.* 94:514–519.

Yang Z. 2007. PAML 4: a program package for phylogenetic analysis by maximum likelihood. *Mol Biol Evol.* 24:1586–1591.

Yang ZH, Nielsen R. 1998. Synonymous and nonsynonymous rate variation in nuclear genes of mammals. *J Mol Evol.* 46:409–418.

Yu BP. 2005. Membrane alteration as a basis of aging and the protective effects of calorie restriction. *Mech Ageing Dev.* 126:1003–1010.

Zwickl D. 2006. Genetic algorithm approaches for the phylogenetic analysis of large biological sequence datasets under the maximum likelihood criterion [Internet]. Austin (TX): The University of Texas at Austin. Available from: http://www.bio.utexas.edu/faculty/antisense/garli/Garli.html